ARL 70-0276
DECEMBER 1970

Aerospace Research Laboratories

CLASSICAL PATH CALCULATIONS OF THE IMPACT BROADENING OPERATOR FOR THE STARK BROADENING OF H_a

M. E. BACON

PLASMA PHYSICS RESEARCH LABORATORY

PROJECT NO. 7073

AIR FORCE SYSTEMS COMMAND

United States Air Force

15

NOTICES

When Government drawings, specifications, or other data are used for any purpose other than in connection with a definitely related Government procurement operation, the United States Government thereby incurs no responsibility nor any obligation whatsoever; and the fact that the Government may have formulated, furnished, or in any way supplied the said drawings, specifications, or other data, is not to be regarded by implication or otherwise as in any manner licensing the holder or any other person or corporation, or conveying any rights or permission to manufacture, use, or sell any patented invention that may in any way be related thereto.

Agencies of the Department of Defense, qualified contractors and other government agencies may obtain copies from the

Defense Documentation Center
Cameron Station
Alexandria, Virginia 22314

This document has been released to the

- - - - - - - - - -

CLEARINGHOUSE
U.S. Department of Commerce
Springfield, Virginia 22151

for sale to the public.

Copies of ARL Technical Documentary Reports should not be returned to Aerospace Research Laboratories unless return is required by security considerations, contractual obligations or notices on a specified document.

200 - MARCH 1971 - CO305 - 29-71-474

ARL 70-0276

CLASSICAL PATH CALCULATIONS OF THE IMPACT BROADENING OPERATOR FOR THE STARK BROADENING OF H_α

M. E. BACON

PLASMA PHYSICS RESEARCH LABORATORY

DECEMBER 1970

PROJECT NO. 7073

AEROSPACE RESEARCH LABORATORIES
AIR FORCE SYSTEMS COMMAND
UNITED STATES AIR FORCE
WRIGHT-PATTERSON AIR FORCE BASE, OHIO

FOREWORD

This report was prepared by Dr. M. E. Bacon under Project 7073 "Research in Plasma Dynamics". The work reported here was performed while the author was a Visiting Research Associate of the Ohio State University Research Foundation, Columbus, Ohio, under Contract F33615-67-C-1758 working in the Plasma Physics Research Laboratory, Aerospace Research Laboratories, Wright-Patterson Air Force Base, Ohio. A briefer paper based on this report has been submitted to the Physical Review for publication. This report contains additional material not heretofore published.

ABSTRACT

Previous classical path calculations of the impact-broadening operator (Φ) for the Stark broadening of the hydrogen line H_α are reviewed. Φ is then computed by solving numerically for the S-matrices using the straight-line-classical path approximation. All contributing multipoles in the perturber-atom interaction V(t) are included and time ordering of the operators in the S-matrices is retained. The resulting Φ matrix elements are compared with the previous approximations. The effects on the H_α line profile are considered.

TABLE OF CONTENTS

LIST OF ILLUSTRATIONS

LIST OF TABLES

INTRODUCTION

The broadening of spectral lines due to the electric microfields in a plasma (Stark broadening) affords a potentially powerful non-interfering probe for the determination of the plasma electron density. In order to effectively utilize this broadening as a probe it is necessary to determine by means of a satisfactory theory, the effects of the microfields on the spectral lines emitted by the plasma. With the development of the generalized quantum mechanical impact theory by Baranger[6] and Kolb and Griem[29] a realistic theoretical formalism for the Stark broadening of spectral lines emitted by a plasma was established. Recently there have been a number of theoretical papers[8] devoted to the Stark broadening of spectral lines which utilize a variety of alternate and more sophisticated formalisms to that given in Reference 6 and 29. However it appears that as far as practical calculations are concerned various approximations must be made which result in expressions for the line profile that differ little from those of References 6 and 29. For this reason and since to date the majority of line profile calculations have been performed using the development of Baranger and Kolb and Griem we shall continue to use their basic framework in this report. We shall be concerned with various modifications to the theory within this framework (in particular modifications to the impact broadening operator Φ) and will confine our attention to the H_α line of hydrogen.

The H_α line of hydrogen lies in the visible region of the spectrum (6563 Å), is well isolated from neighboring lines and is subject to the large linear Stark effect characteristic of the hydrogen lines. H_α is the simplest hydrogen line in the visible region of the spectrum with an "unshifted" central component and a profile sensitively dependent on the effects of the free electrons in the plasma. It is therefore attractive as an easily accessible line for the study of these effects. Furthermore for electron densities between 10^{17} e/cm^3 and 10^{18} e/cm^3, H_α becomes a prime candidate for use in electron density determinations since at these densities the widely used H_β line is appreciably distorted by overlap with the neighboring H_ε line. Until recently a major drawback in the study of the H_α line and its usefulness as a diagnostic tool has been the rather pronounced self absorption. Recent experimental advances[13] however have made it possible to extract reliable experimental H_α profiles from a pure hydrogen plasma exhibiting self absorption through an iterative series of integrations and "Abel inversions"[12]. In addition, recent theoretical and experimental advances make H_α extremely attractive for use as a diagnostic tool in "seeding" experiments provided due care is taken with regard to possible demixing phenomena.

The first calculations of the H_α line profiles using the theory developed in references 6 and 29 were performed in 1959 by Griem, Kolb and Shen[19] (GKSI) (other lines of Lyman and Balmer series were calculated but these will not concern us here).

In most cases these GKSI profiles have 10 - 20% smaller half-widths than the experimentally determined profiles[9,11,14,25,32]. In 1968 Bacon and Edwards[2,3], (BE) performed calculations of the GKSII[22] type for the H_α line which agree very well with the experimental results. At about the same time Kepple and Griem[28] (KG) incorporating a number of modifications to the GKSI and GKSII formalisms[20], also found improved agreement with experiment. An analysis of these calculations[4] confirmed the consistency of the BE and KG calculations within their respective approximations, and also indicated that for the case of H_α strong collisions and in general variations of the electron broadening operator have a significant effect on the line profile. This together with additional analysis (See Section III of this report) tends to make suspect the inconsistent and at times arbitrary treatment of the strong collisions made in References 2, 3, and 28. Furthermore, recent calculations pertaining to the Lyman-α line[5] indicate that estimates of strong collision corrections and corrections due to higher order multipoles in the electron atom interaction used in the above mentioned calculations may well be in error and could significantly affect the line profile. In view of the above considerations the agreement between experiment and theory obtained heretofore could quite easily be accidental.

The purpose of this report therefore is to eliminate the inconsistencies in the previous classical path calculations by numerically calculating the S-matrices used to calculate the impact broadening operator Φ, retaining the correct time ordering and including all

contributing multipoles in the free electron atom interaction in the same manner as was done for the Lyman-α[5] line. The resulting ϕ - matrix elements are compared with the previous calculations and the effects on the line profile considered.

The previous calculations of the ϕ- matrix have varied in a number of ways which makes comparison with the present calculations rather difficult. In particular the cut off at large impact parameters (ρ_{max}) and the treatment of lower state broadening has varied significantly amongst the previous calculations. (These differences are described in some detail in Section III). Since the effects of the modifications to the theory presented in this report manifest themselves through higher order terms in the iterative solution (Dyson expansion) for the S-matrices* or in physical terms arise from collisions with small impact parameters considerations of variations in the upper impact parameter cut off will not concern us here. It should be noted however that the upper cut offs used in the previous calculations have all been taken in the vicinity of the Debye radius (ρ_D), and we shall consistently use $\rho_{max} = \rho_D$ in Section IV when comparing the various calculations. In addition the complete $\mathcal{R}$ matrix (Eq. 20) is used (some previous calculations have neglected various terms of $\mathcal{R}$: see Section III). In making the comparison in Section IV, we have continued to characterize the previous calculations as GKSI[19],

*Previous calculations have considered only terms up to second order in the interaction V(t).

BE(GKSII)[3], SC[34], and KG[28] which is indicative of the particular treatment of close collisions in each calculation rather than of the calculations themselves. The line profiles presented in Section IV are therefore of a relative nature.

The ϕ-matrix elements can be compared as succinctly as possible by specifying the "constants" K (Eq. 20) in the same manner as was done for Lyman-α . These constants are absolute and are independent of variations in ρ_{max}. Detailed calculations of the H_α profiles as a function of electron density and temperature using the results of this report are presently underway.

The following section contains an outline of the formalism and notation, followed in Section III by a review of previous calculations. Section IV contains the results of the present calculations and a comparison with previous calculations. This is followed by a summary and discussion in Section V and finally by a list of references in Section VI.

II. FORMALISM AND NOTATION

Using the generalized theory developed in References 6 and 29 the line profile for a hydrogen line, in reduced units α (see for example Reference 21) may be written:

$$S(\alpha) = A_{nn'}/\pi \int_0^\infty W_r(f)\, df\, \mathrm{Re}\langle \eta|\mu|S\rangle\langle \eta S|\sigma'|S'\eta'\rangle\langle \eta'|\mu|S'\rangle. \qquad (1)$$

$\eta\eta'$-----, and $\xi\xi'$----- each represent a set of quantum numbers characterizing an eigenstate (to 1st order) of a hydrogen atom in a static electric field (ion microfield f). These eigenstates are the parabolic wave functions[10] represented by a set of three quantum numbers $|n_1 n_2 m>>$. The notation $|\xi,\eta>>$ is due to Baranger[6] and denotes a state of the "doubled atom" each state of which corresponds to two states of the original atom, one (η) from the upper levels with principal quantum number n and the other (ξ) from the lower levels with principal quantum number n'. When referring to a specific state of this system we shall use the notation $|n_1' n_2' m'; n_1 n_2 m>>$. $W_r(f)$ is the ion-field distribution function. The distribution functions of Hooper[28] will be used throughout this report. μ is the appropriately weighted[6,29,36] scalar dipole moment operator and $A_{nn'}$ is a normalization factor such that $\int S(\alpha)d\alpha = 1$

$$\text{i.e.,} \qquad A_{nn'} = 1/\sum_{\eta\xi} |<\eta|\mu|\xi>|^2 \tag{2}$$

$$O = i\lambda_o^2[\omega - (H_n(f) - H_{n'}(f))/K]/2\pi C F_o + \Phi_{nn'} \tag{3}$$

λ_o is the unshifted wavelength and $F_o = 2.61eN^{2/3}$ is the normal Holtzmark field strength in c.g.s. units. N is the electron density. H(f) is the Hamiltonian for a hydrogen atom in a static field f. The subscripts n, n' indicate that H(f) acts on the upper (η,η'-----) or lower (ξ,ξ'-----) states, respectively.

The operator $\Phi_{nn'}$ contains the effects of the free electrons on the line profile and is of major importance as far as this report is concerned. Apart from differences in the ion-field distribution function (ie., the ion-field distribution functions of Ecker[17], Mozer and Baranger[31], Hooper[26]), the calculated profiles to date have differed mainly in the treatment of this operator which we shall now define.

$$\Phi_{nn'} = -(\lambda_0^2 N^{1/3}/2.61ec)\int v f(v) dv \int \rho d\rho \left\{ S_n^* S_{n'} - 1 \right\}_{av.} . \tag{4}$$

ρ is the impact parameter (distance of closest approach) of the perturbing electron and v is the electron speed. f(v) is the speed distribution function (assumed to be Maxwellian). S_n and S_n' are given by

$$\begin{aligned} S_n &= U_n(\infty,-\infty), \\ S_{n'} &= U_{n'}(\infty,-\infty), \end{aligned} \tag{5}$$

where U_n and $U_{n'}$ are the time development operators, in the interaction representation for states with principal quantum number n and n', respectively. U satisfies the equations,

$$\begin{aligned} i\hbar \frac{\partial U}{\partial t} &= \tilde{V}(t) U , \\ U(-\infty,-\infty) &= I . \end{aligned} \tag{6}$$

The approximation inherent in the assumption, implied above, that we need concern ourselves with U acting only between states of the same principal quantum number is the usual no quenching approximation. In this approximation we assume that we may neglect transition between states with different principal quantum numbers caused by the perturbing electrons in comparison to transitions between states with the same principal quantum number. This should be a good approximation for transitions involving low lying atomic levels such as the levels involved in the H_α emission process but not for n and n' large[23]. It should be noted that in solving Eq. (6) for U_n and $U_{n'}$ a sum over a complete set of states is implied on the R.H.S. even though we are only interested in elements of U between states of the same principal quantum number on the L.H.S.

In the classical path approximation (see for example Ref. 35) $\tilde{V}(t)$ is given by

$$\tilde{V}(t) = \exp[i H(f) t/\hbar]\, V(t) \exp[-i H(f) t/\hbar] \,. \tag{7}$$

V(t) is the classical interaction between the perburbing electron and the hydrogen atom.

Equation (6) may be solved by iteration yielding,

$$S = U(\infty,-\infty) = 1 - (i/\hbar)\int_{-\infty}^{\infty} \tilde{V}(t_1)\,dt_1 + (i/\hbar)^2 \int_{-\infty}^{\infty} \tilde{V}(t_1)\,dt_1 \int_{-\infty}^{t_1} \tilde{V}(t_2)\,dt_2 + \cdots \,. \tag{8}$$

The presence of the exponentials in Eq. (7) which are functions of the ion field f make the evaluation of Eq. (8) exceedingly difficult without further approximation. This is because one has a preferred direction in space, due to f, and the average in Eq. (4) cannot easily be accomplished. For this reason it is usual to replace H(f) in Eq. (7) by the Hamiltonian of the unperturbed hydrogen atom. For convenience and because the transformation from spherical wave functions to parabolic wave functions is well known[27] (see also Appendix A) we shall work with spherical wave functions when determining $\phi_{nn'}$ and transform to the parabolic system when calculating the profile (S(α)). With this in mind we may split the R.H.S. of both Eqs. (6) and (8) into terms involving a sum over states with the same principal quantum number and terms involving a sum over states with different principal quantum number. Since the hydrogen atom is degenerate we may then replace $\tilde{V}(t)$ by V(t) in the terms involving a sum over states with the same principal quantum number, while the terms involving a sum over states with different principal quantum numbers vanish because of the rapid oscillation of the exponentials over the times of interest in these terms. This is certainly a good approximation for low temperatures and large impact parameters but is somewhat questionable for small impact parameters particularly at high temperatures. For a further discussion of this point the reader is referred to reference 35, page 415. We may now write Eq. (6) in the form,

$$i\hbar \frac{\partial U}{\partial t} = V(t) U \qquad (9)$$

and Eq. (8),

$$S = U(\infty,-\infty) = 1 - (i/\hbar)\int_{-\infty}^{\infty} V(t_1)dt_1 + (i/\hbar)^2 \int_{-\infty}^{\infty} V(t_2)dt_2 \int_{-\infty}^{t_2} V(t_1)dt_1 + \cdots \quad (10)$$

with the understanding that the R.H.S. of (9) and (10) only involves a sum over states with the same principal quantum number. Because of this limited sum on the R.H.S., $V(t_1)$ does not commute with $V(t_2)$ and it is not permissible to write (10) in the form of an exponential. (This approximation was made in Refs 34,20). We note, however, that to second order in V(t) we may write (10) in the form of an exponential since the time integration makes the integral of the "reduced commutator" zero anyway.

In the following sections we shall be referring to a number of explicit expressions for $\{S_n^* S_n - 1\}$ av. which we shall now briefly consider. Derivations for these expressions may be found elsewhere in the literature (see for example Reference 21). Keeping only the dipole term in the multipole interaction for a free electron interacting with a hydrogen atom, V(t) may be written,

$$V(t) = -\frac{e^2 \vec{r}\cdot\vec{R}}{|\vec{R}|^3} \quad (11)$$

or equivalently

$$V(t) = -e^2 r P_1(\cos\theta')/|\vec{R}|^2 \quad (12)$$

where $\vec{R} = \vec{\rho} + \vec{v}t$

(The coordinate system is the same as that defined in Appendix B). (11) and (12) are strictly valid only for $R \gg r$. Substituting into Eq. (10), solving for S_n^* and $S_{n'}$ and retaining only terms up to and including 2nd order in $V(t)$, $\{S_n^* S_{n'} - 1\}_{av.}$ may be written[21],

$$\left\{S_n^* S_{n'} - 1\right\}_{av.} = -2[r_n \cdot r_n + r_{n'} \cdot r_{n'} - 2r_n \cdot r_{n'}]/3\rho^2 , \qquad (13)$$

where r_n and $r_{n'}$ are in atomic units and ρ is in units of $\hbar/mv$.

When the lower state is unperturbed (one-state case) $S_{n'} = I$ and

$$\left\{S_n^* S_{n'} - 1\right\} \rightarrow \left\{S_n^* - 1\right\}_{av.} = -2[r_n \cdot r_n]/3\rho^2 . \qquad (14)$$

Substituting (13) or (14) into Eq. (4) and performing the integrations over ρ and v one obtains,

$$\Phi = C\,[E_1(y_{min})]\,\mathcal{R} , \qquad (15)$$

where $\mathcal{R}$ is $[r_n \cdot r_n + r_{n'} \cdot r_{n'} - 2r_n \cdot r_{n'}]$ or $[r_n \cdot r_n]$ respectively.

$$C = -\lambda_0^2 \hbar^2 N^{1/3} (2m/RT)^{1/2}/(2.61 \text{ec m}^2) , \qquad (16)$$

$$\text{and } E_1(y_{min}) = -\gamma - \ln(y_{min}) - \sum_{n=1}^{\infty} (-1)^n y_{min}^n / n\,n! , \qquad (17)$$

$$y_{min} = (4\pi N/3m)(e\hbar n^2/kT)^2 . \qquad (18)$$

In the limit y_{min} small (<0.1)

$$E_1(y_{min}) = -\gamma - \ln(y_{min}) . \tag{19}$$

In performing the ρ integration we have used an upper cut off of ρ_D and a lower cut off of $(2/3)^{\frac{1}{2}}\, n^2\hbar/mv$ in accordance with GKSI[19].

Analogous to Eq. (15), with $\mathcal{R}$ equal to $[r_n \cdot r_n + r_{n'} \cdot r_{n'} - 2r_n \cdot r_{n'}]$, we may conveniently compare the ϕ matrix elements of the various calculations by specifying the constants K in the following equation:

$$\Phi = C[E_1(y_{min}) - K]\mathcal{R} . \tag{20}$$

GKSI is rather a special case since for some ϕ matrix elements $[r_n \cdot r_n + r_{n'} \cdot - 2r_n \cdot r_{n'}]$ was used and for others $[r_n \cdot r_n]$ (see the following section). Similarly the BE calculations did not use the complete $\mathcal{R}$ matrix[3].

In concluding this Section we shall briefly consider the approximations one makes in arriving at some of the equations of this section. For an in depth study of these approximations the reader is referred to a number of reviews[21,35,7]. In arriving at Eq. (1) with $\phi_{nn'}$ defined by (4) we have made the quasi-static approximation for the treatment of the ions and the impact approximation for the treatment of the electrons. In addition we have made the no quenching assumption already mentioned. Obviously there will be some ions in the tail of the Maxwellian distribution which will be moving fast enough to be considered under the impact

approximation and conversely a number of electrons in the head of the distribution which are moving slow enough to be considered by the quasi-static approximation. The number of such ions and electrons, and their relative importance, will, of course, be dependent on the frequency separation from the line center. With these reservations we note that the usual validity criteria (see for example 19 and 37) for the above mentioned approximations, derived using nominal values for interaction times, etc., are well satisfied for that portion of the line profile we shall consider in this report (i.e., the center and near wings). In arriving at Eq. (6) with $\tilde{V}(t)$ defined by (7), we have made the classical path approximation. A review of classical path methods, as applied to the problem of line broadening, has recently been given by Smith, et. al.,[35] and will not be discussed further.

III PREVIOUS CALCULATIONS

(a) GKSI Type:

Until recently the only readily available H_α profile calculations for use in plasma diagnostics were those of Griem, Kolb, and Shen[19]. In the following we shall briefly outline the treatment of the electron impact operator Φ_{32} used by these authors, and present explicit expressions for the relevant elements of the operator part of Φ_{32} viz $\{S_3^* S_2 - 1\}_{av.}$. As mentioned in the previous section, we will, for convenience, be evaluating this operator in terms of the basis states $\{|n\ell m\rangle\}$, since this allows us to compare as succinctly as possible the different calculations. When necessary, however, we will also make use of the basis states $\{|n_1 n_2 m\rangle\}$; and the reader should exercise due caution in this respect.

In GKSI the matrix elements of Φ_{32} were evaluated in the following manner: Only the dipole term in the free electron atom interaction (i.e., Eqs. 11 or 12) was considered. Lower state broadening was neglected except when considering the broadening of the central unshifted components of the Stark pattern. As far as the shifted components are concerned, we need consider only the one state case Eq. 14. Furthermore, Eq. 15 of Ref. 34 shows us that the only non-zero terms are the diagonal components and that the value of $\{S_3^* - 1\}_{av.}$ is independent of m for a given ℓ (see also Baranger[6]). Hence, for the unshifted components, we need only consider the following three explicit expressions:

$$\langle 300|\{S_3^*-1\}_{av.}|300\rangle = -108/\rho^2 \qquad \text{(i)}\ ,$$

$$\langle 31m|\{S_3^*-1\}_{av.}|31m\rangle = -81/\rho^2 \qquad \text{(ii)}\ , \qquad (21)$$

$$\langle 32m|\{S_3^*-1\}_{av.}|32m\rangle = -27/\rho^2 \qquad \text{(iii)}\ .$$

These may be derived by using Eq. (14) of the previous Section or alternatively by applying the transformation given in Appendix A to the $r_3 \cdot r_3$ matrix elements given for example in Ref. 3.

In terms of the parabolic states, the elements of Φ_{32} corresponding to the unshifted components are,

$$\ll 110;00\pm1|\Phi_{32}|00\pm1;110\gg$$

and $$\ll 00\pm2;00\pm1|\Phi_{32}|00\pm1;00\pm2\gg$$

In the case of the former, we require the following elements of $\{S_3^*S_2-1\}_{av.}$ in terms of the spherical wave functions:

$$\ll 300;21\pm1|\{S_3^*S_2-1\}_{av.}|21\pm1;300\gg = -114/\rho^2 \qquad \text{(i)}\ ,$$

$$\ll 310;21\pm1|\{S_3^*S_2-1\}_{av.}|21\pm1;310\gg = -87/\rho^2 \qquad \text{(ii)}\ , \qquad (22)$$

$$\ll 320;21\pm1|\{S_3^*S_2-1\}_{av.}|21\pm1;320\gg = -33/\rho^2 \qquad \text{(iii)}\ ,$$

and in the case of the latter we require only,

$$\ll 32\pm2;21\pm1|\{S_3^*S_2-1\}_{av.}|21\pm1;32\pm2\gg = -33/\rho^2\ . \qquad (23)$$

That (22) and (23) are the only elements of consequence as far as the unshifted components are concerned may be established by considering the two-state transformation of Appendix A applied to the $[r_n \cdot r_n + r_{n'} \cdot r_{n'} - 2r_n \cdot r_{n'}]$ matrix of Ref. 3. The results may be checked by keeping only the first two terms of the cosines for the elements in rows 20, 21, 23, and 25 of Table CI, Appendix C.

All these elements above show the usual divergence as $\rho \to 0$ and as $\rho \to \infty$. The divergence at large impact parameters is treated in the GKSI calculations by cutting off the ρ integration at $\rho_{max} = \rho_D$ where ρ_D is the Debye length. The divergence at small impact parameters resulting from the neglect of higher order terms in the Dyson expansion for S_n and $S_{n'}$ (Eq. 10) is handled by defining a minimum impact parameter ρ_{min} with the help of the condition:

$$|\{S_3^* S_2 - 1\}_{av.}| = 1 \qquad (24)$$

corresponding to practically complete destruction of the correlation between states of the system before and after collisions[21,6].

The strict application of condition (24) to the expressions (21), (22), (23) results in a ρ_{min} ranging from 10·7 - 5·2 in units of $\hbar/mv$. In the GKSI calculations a nominal value of ρ_{min} was chosen, given by,

$$\rho_{min} = (2/3)^{1/2} n^2 (\hbar/mv) = 7.35 (\hbar/mv) \qquad (25)$$

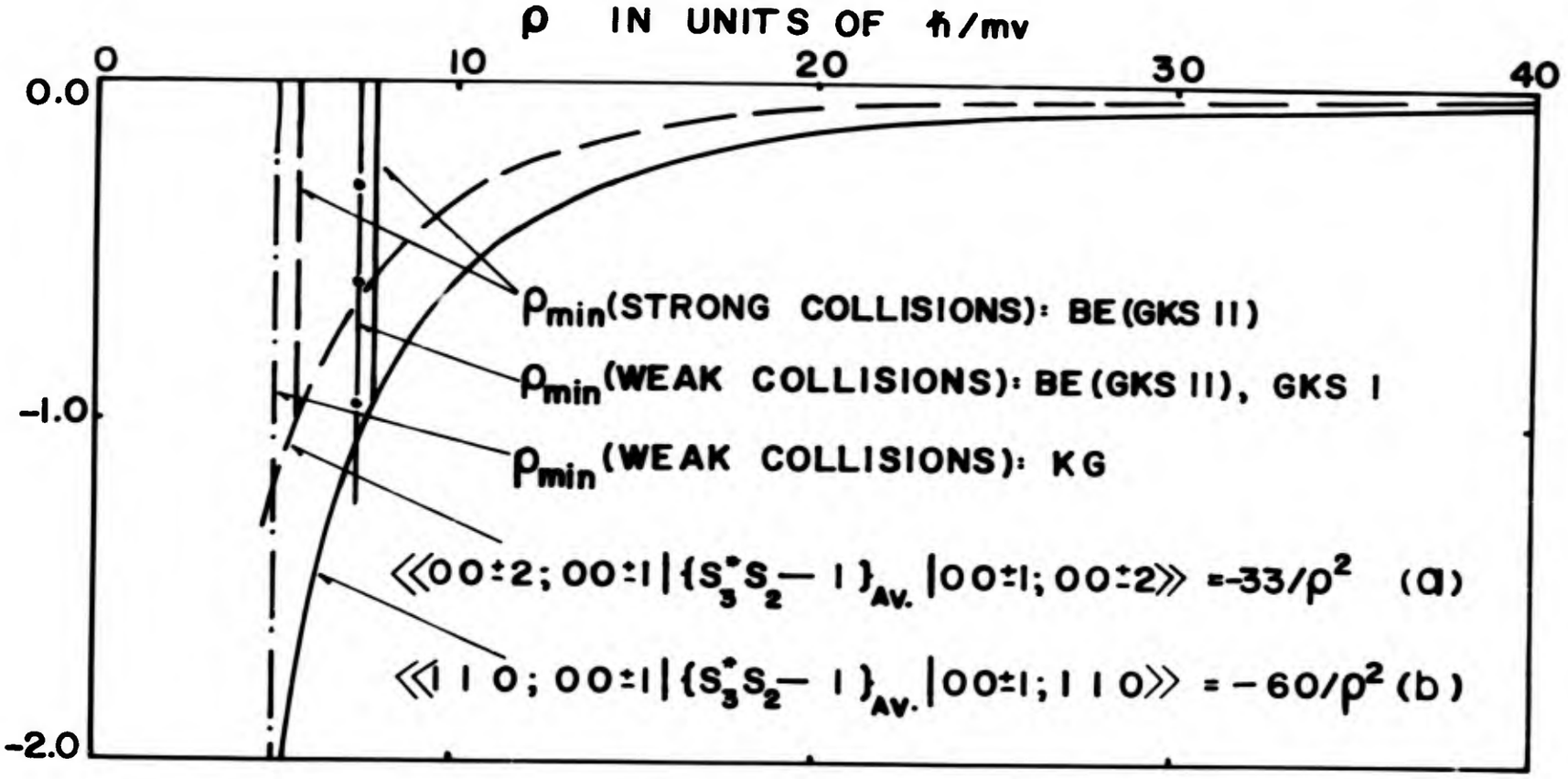

Fig. 1. Φ_{32} for the unshifted central components as a function of ρ. Also shown are the ρ_{min} cut offs used in various calculations.

In Fig. 1 we have plotted the operator part of Φ_{32} for the unshifted components (in terms of parabolic wave functions), as a function of ρ in units of $\hbar/mv$. We have indicated the ρ_{min} cut-off for the strict application of condition (25) by the solid line. We note that using the GKSI cut-off we underestimate the value of component (a) and slightly overestimate the value of component (b). There is no valid reason for choosing ρ_{min} defined by (25) over ρ_{min} defined by the strict application of (24) or vice versa since (24) is in the first place approximate, except perhaps that the strict application of (24) is more consistent. The futility of trying to improve the reliability of the theoretical calculations of any theory that employs condition (24) in lieu of taking higher order terms in the Dyson expansion is illustrated in Fig. 2. Curve (a) shows the H_α profile $S(\alpha)$ for $N = 10^{17}$ e/cm^3 and $T = 2 \times 10^{4^\circ}$K with the strict application of the condition (24), while curve (b) is the GKSI curve using the nominal ρ_{min} (Eq. 25). Curve (a) is seen to be some 10% broader than curve (b). Since (24) serves only as a guide to a choice of ρ_{min}, one must conclude that curves (a) and (b) are equally valid. In fact, one is faced with the possibility of fitting all the experimental data merely by a "proper" choice of ρ_{min} somewhere between 5 and 10. We shall see that the recent calculations of the H_α profile by Bacon and Edwards and Kepple and Griem suffer from the same drawback and therefore that the agreement obtained between theory and experiment must necessarily be fortitious.

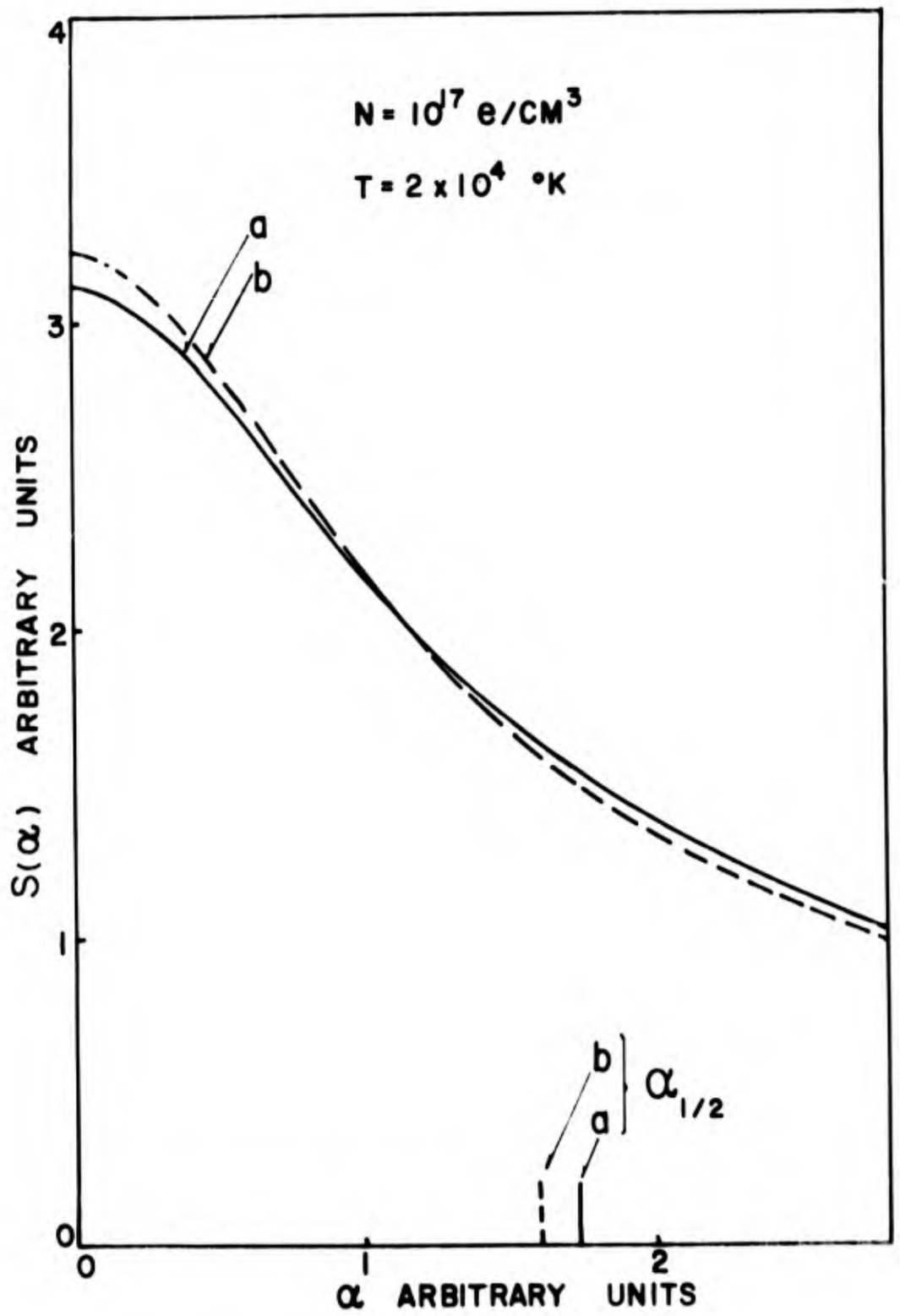

Fig. 2. Comparison of the H_α profile (a) using ρ_{min} (weak collisions) = ρ_{min} (strong collisions) and (b) using Eq. 25 for the weak collisions and condition (24) for the strong collisions.

(b) GKSII Type:

Recently Bacon and Edwards [2,3] performed calculations similar to those performed by Griem, Kolb, and Shen for the H_β line. Formally, these calculations considered lower state broadening of all components of the line, keeping only the dipole term in the free electron atom interaction and including a strong collision term for those collisions with impact parameter $0 < \rho < \rho_{min}$, where ρ_{min} was defined by Eq. (24). The ρ integration in Eq. (4) was split into two parts. $|\{S_3^* S_2 - 1\}|_{av.}$ was set equal to 1 for $0 < \rho < \rho_{min}$ (strong collisions) and equal to Eq. 13 for $\rho_{min} \leq \rho \leq 1.12\ \rho_D$ (weak collisions). An upper cut-off at $1.12\ \rho_D$ suggested by Griem, et. al.[24], was used. In practice, these formal considerations were applied in a somewhat inconsistent manner, in order to facilitate a savings in computer time, on the assumption that these inconsistencies would have little effect. In view of the sensitive effect of Φ on the profile, these approximations must necessarily be viewed with suspicion (see Ref. 4). First: Certain elements of $[r_3 \cdot r_3 + r_2 \cdot r_2 - 2 r_3 \cdot r_2]$ were neglected[3]. These elements can have a significant effect on the half width, as pointed out in Ref. 4. In fact, in certain instances, the inclusion of lower state broadening, without other modifications to the GKSI calculations (i.e., neglecting strong collisions and taking ρ_{max} to be ρ_D), results in a narrowing of the line (in this respect see Mineva[30] and Baranger[7], page 525)

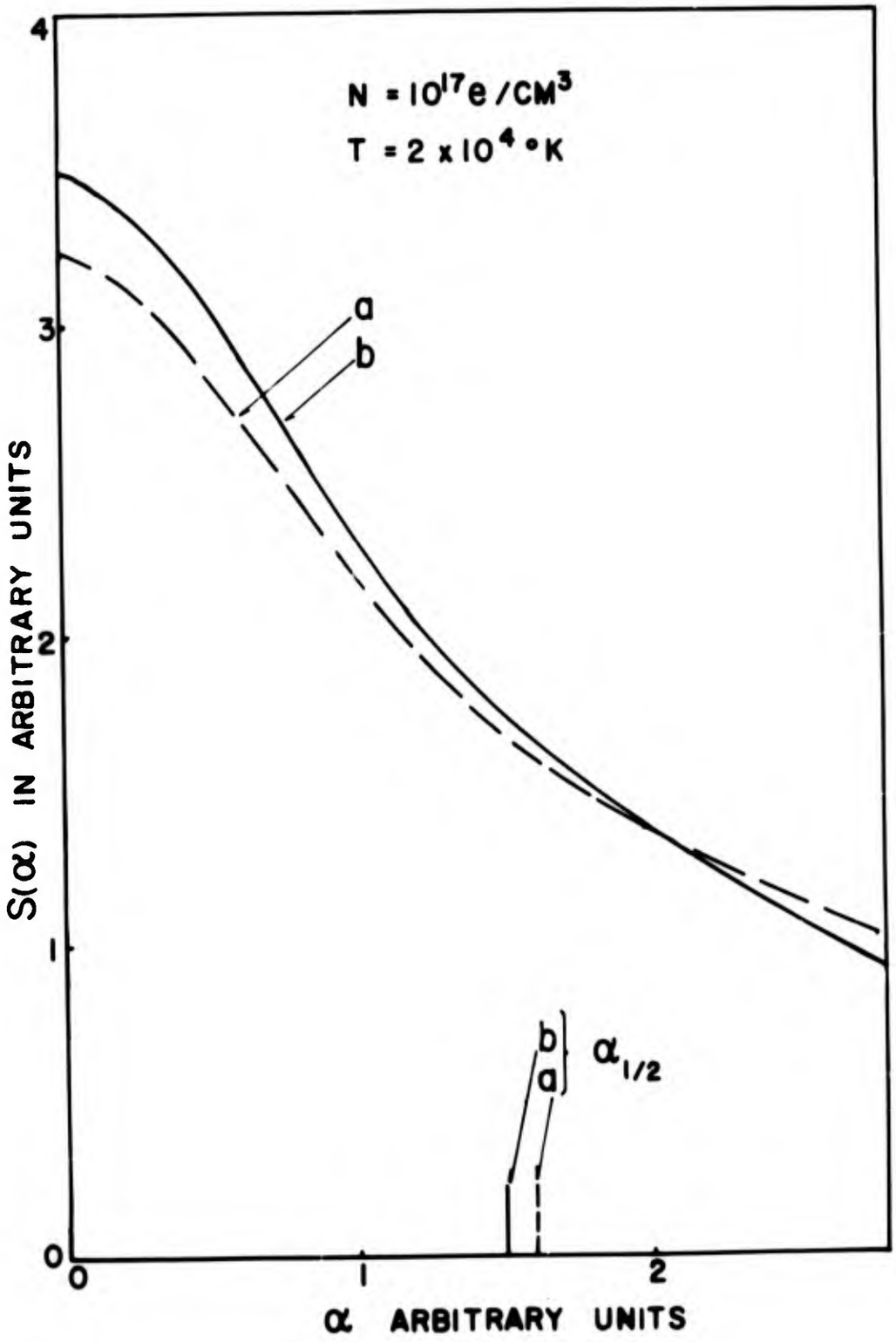

Fig. 3. Comparison of the H_α profile (a) including lower state broadening of only the central unshifted components (GKSI) and (b) including complete lower state broadening.

This is demonstrated in Fig. 3 for an electron density of $N = 10^{17}$ e/cm^3 and a temperature of $T = 2 \times 10^{4°}$K. Curve (a) is the GKSI curve and curve (b) is the curve with the inclusion of all lower state broadening, including all the cross terms. Second: ρ_{min} was chosen consistently when treating the strong collision; but the nominal value of Eq. (25) was used when treating the weak collision. The effect of this has already been demonstrated in the previous section. It is apparent that there again exists the possibility of choosing from a number of equally valid ρ_{min}'s and thereby fitting the experimental data. Apparently the inconsistent, and at the same time, valid (valid in the sense that any ρ_{min} between 5 - 10 is permissible using the approximate condition (24)) choice made in the BE calculations fits the available data very well. Other choices of ρ_{min} are permissible which could, however, cause quite substantial disagreement.

(c) KG Calculations:

In 1968 Kepple and Griem[28] performed calculations for a number of hydrogen lines. We will be concerned only with their treatment of H_α; and much of the specifics of what follows may not apply to to the other lines they considered.

In the KG calculations Eq. (13) was used for the operator part of Φ. Complete lower state broadening was included and, using condition (19) as a guide, ρ_{min} was chosen to be:

$$\rho_{min} = (n^2 - n'^2)(\hbar/mv) \qquad (26)$$
$$= 5.(\hbar/mv)$$

All other things being equal, the lowering of the minimum impact parameters to 5 results in an increase in the halfwidth of $\sim$ 10% (see reference 15, page 320). As already demonstrated in the subsection on the GKSI calculations, changes in the halfwidth of this order due to changes of ρ_{min} are to be expected (see Fig. (2)). This again demonstrates the unsatisfactory nature of the arbitrary cut-off procedure used at small impact parameters.

With ρ_{min} defined as above, KG add a strong collision term of-0.4. This term was carried over directly from the work of Griem[20] who, by assuming that the free electron interaction commutes with itself at different times, was able to sum the first 10 terms of the Dyson expansion for the Lyman-α line*. This term, together with the reduction of ρ_{min}, effectively produces a strong collision term of-0·78†. It is difficult to justify the application of the Lyman-α results to H_α; and there seems to be little to recommend this procedure over that used in the BE calculations. In addition, it is worth noting at this point

*In the case of L-α the term-0.4 was added to the GKSI results with ρ_{min} defined by Eq. (25).

† -.4 - ln (ρ_{min} defined by (26) divided by ρ_{min} defined by (25)).

that extending the Shen-Cooper[34] formalism* to the two-state case (see Appendix C) results in strong collision corrections ranging from-0·724 to 0·983 (table C1) - quite different from Lyman-α[20,34].

KG also add a quarupole term-$8kT/3E_H$ which is again carried over directly from the Lyman-α work of Griem[20]. Combining this with the-0·78 above, we find a "strong collision correction" of -0·95 at $10^{4°}$K and-1.46 at $4 \times 10^{4°}$K - at low temperatures remarkably close to the strong collision correction used by BE.

In addition, KG introduce modifications which account, in an approximate way, for the effect of ion-field splitting and the finite duration of the collisions. To do this they choose a ρ_{max} to be the minimum of v/w_c or ρ_D where $w_c = \max(\Delta w_o, \Delta w_s)$. Δw_o corresponds to the Lewis cut-off and Δw_s is of the order of the ion field splitting. In the center and near wings Δw_s is generally the larger of the two and is estimated to be,

$$\Delta w_s \cong 5n^2 k N^{2/3}/m \equiv w_c \qquad (27)$$

ρ_{max} is then chosen to be the minimum of,

$$vm/(5kn^2N^{2/3}) \quad \text{or} \quad \rho_D$$

*The procedure of Griem[20] is exactly equivalent to that of Shen and Cooper. The procedure of Shen and Cooper, however, is applicable to any line and relatively easy to extend to the two-state case (lower state broadening).

An averaging process was then adopted (see KG, Eq. (13)) to try and minimize errors in (27). The error involved in this choice of ρ_{max}, is, according to Eq. (14) of KG (see also Ref. 4), estimated to be much smaller than the errors involved in the "strong collision correction".

It is difficult to judge what effect the cut-off due to the ion field splitting has on the line profile since Eq. (27) is at best approximate. However, assuming (27) is valid, and taking a nominal perturber velocity $v = (2KT/m)^{1/2}$, we find that

$$v/w_c < \rho_D \text{ for } N > 10^{19} \text{ e/cm}^3$$

In other words, $\rho_{max} = v/\Delta w_s$ should be used instead of $\rho_{max} = \rho_D$ only for $N > 10^{19}$ e/cm^3. Obviously, for a given density and temperature, there will be some electrons with v small enough so that $\rho_{max} = v/\Delta w_s$ should be used instead of ρ_D and, of course, the uncertainty in Eq. (27) further weakens the condition on N obtained above. It is, however, probably safe to say that the ion field splitting is not very significant in the case of H_α below $N \gtrsim 10^{18}$ e/cm^3.

(d) Conclusion:

The purpose of the preceeding three subsections has been to present a brief outline of the treatment of the impact broadening operator used in previous calculations in such a manner as to illustrate the inconsistent and, at times, arbitrary treatment of the electron broadening in an attempt to establish the motivation

for the present calculations. The agreement obtained heretofore with experiment, in view of the preceeding analysis, is probably accidental; and the theoretical situation is at best unsatisfactory. The calculations presented in the following section, we believe, remove much of the uncertainty associated with close collisions and improve the consistency of the classical path Stark broadening theory, as applied to H_α.

IV PRESENT CALCULATIONS

In this section we present calculations of the electron impact broadening operator Φ, using the straight line classical path approximation and compare these with previous calculations based on the same approximation; i.e., GKSI, BE (GKSII), SC, and KG. All contributing multipoles in the perturber (electron) atom interaction (V(t)) are considered; and the S-Matrices (Eq. 10) are determined numerically by solving for the time development operator in the interaction representation (Eq. 9) preserving the correct time ordering.

The relevant V(t) matrix elements are given in Appendix B for the n = 3 and n' = 2 levels. The set of coupled equations

$$i\hbar\frac{\partial}{\partial t}\langle n\ell m|U|n\ell'm'\rangle = \sum_{\ell''m''}\langle n\ell m|V(t)|n\ell''m''\rangle\langle n\ell''m''|U|n\ell'm'\rangle \qquad (28)$$

for n = 2 has already been solved for the case of L-α considered in reference 5. A similar set of equations for the n = 3 levels, using the matrix elements given in Table BII and BIII, were integrated numerically from $t \tilde{=} -\infty$ to $t \tilde{=} \infty$ with the initial condition

$$u(-\infty,-\infty) = I \qquad (29)$$

for various values of electron speed v and impact parameter ρ^*. The average $\{S_3^* S_2 - 1\}$ av. over perturber parameters (angular

*The coordinate system, the so-called collision axes, is defined in Appendix B.

average) was then calculated as a function of ρ and v, using equation C1 of Appendix C.

Four elements of the $\{S_3^* S_2 - 1\}$ av. matrix are shown plotted in Figs. 4-7 as a function of ρ for the perturber speed v = 0.35 (a.u.). The first three are the elements of interest as far as the weaker of the two "unshifted" components of H_α is concerned, while Fig. 7 is the relevant element for the strongest "unshifted" component. Shown for comparison are the curves used by BE (GKSII) and KG, and the curve calculated using the formalism of Shen and Cooper[34] (SC). In addition, we also show the "dipole only" curve. For the case of the BE (GKSII) curves, we show the weak and strong collision cut-offs*. The BE (GKSII), SC, and "dipole only" curves are independent of v, while the present curves depend on v. The "dipole only" curve, as in the case of Lyman-α[5], is obtained by setting all the multipole terms in the free electron atom interaction equal to zero except for the dipole terms. In addition,

*The weak cut-off is the minimum impact parameter cut-off for the weak collisions - the nominal value for which $|\{S_3^* S_2 - 1\}av.| = 1$; i.e., ρ min = $(2/3)^{1/2} n^2$. The strong collision cut-off is the maximum impact parameter for the "strong collisions" which varies from element to element and is given by ρ min = $|2/3\mathcal{R}|^{1/2}$.

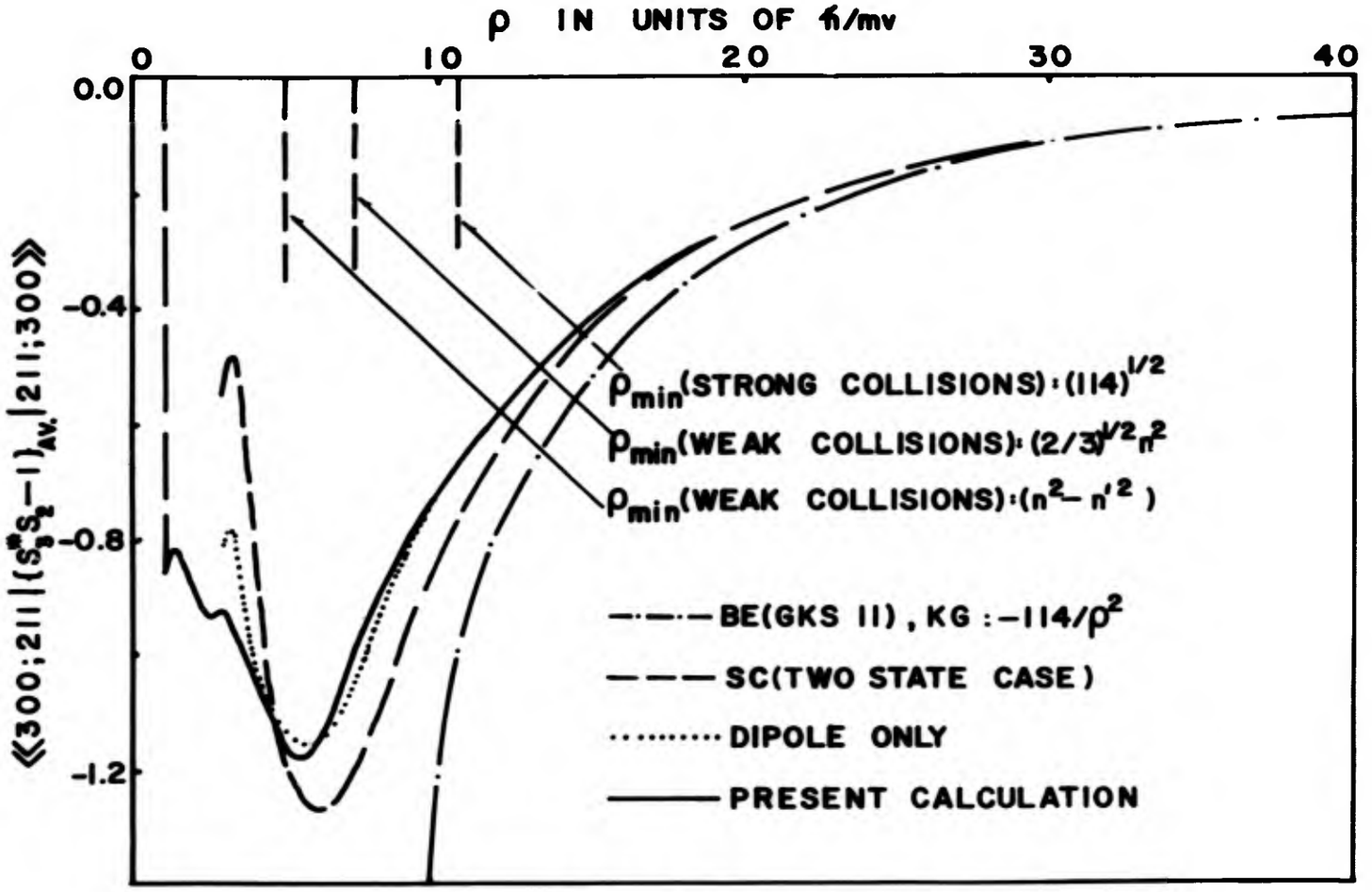

Fig. 4. Typical $(S_3^* S_2 - 1)_{av.}$ matrix element as a function of ρ using various approximations. The curves derived in the present calculations are functions of v. The particular curve shown is for $v = 0.35$ or $X = \hbar/mva_0 = 1/0.35$. The BE(GKSII), KG, SC and dipole only curves are independent of v and are shown for comparison. Also shown are the ρ_{min} cut offs used in BE(GKSII) and KG.

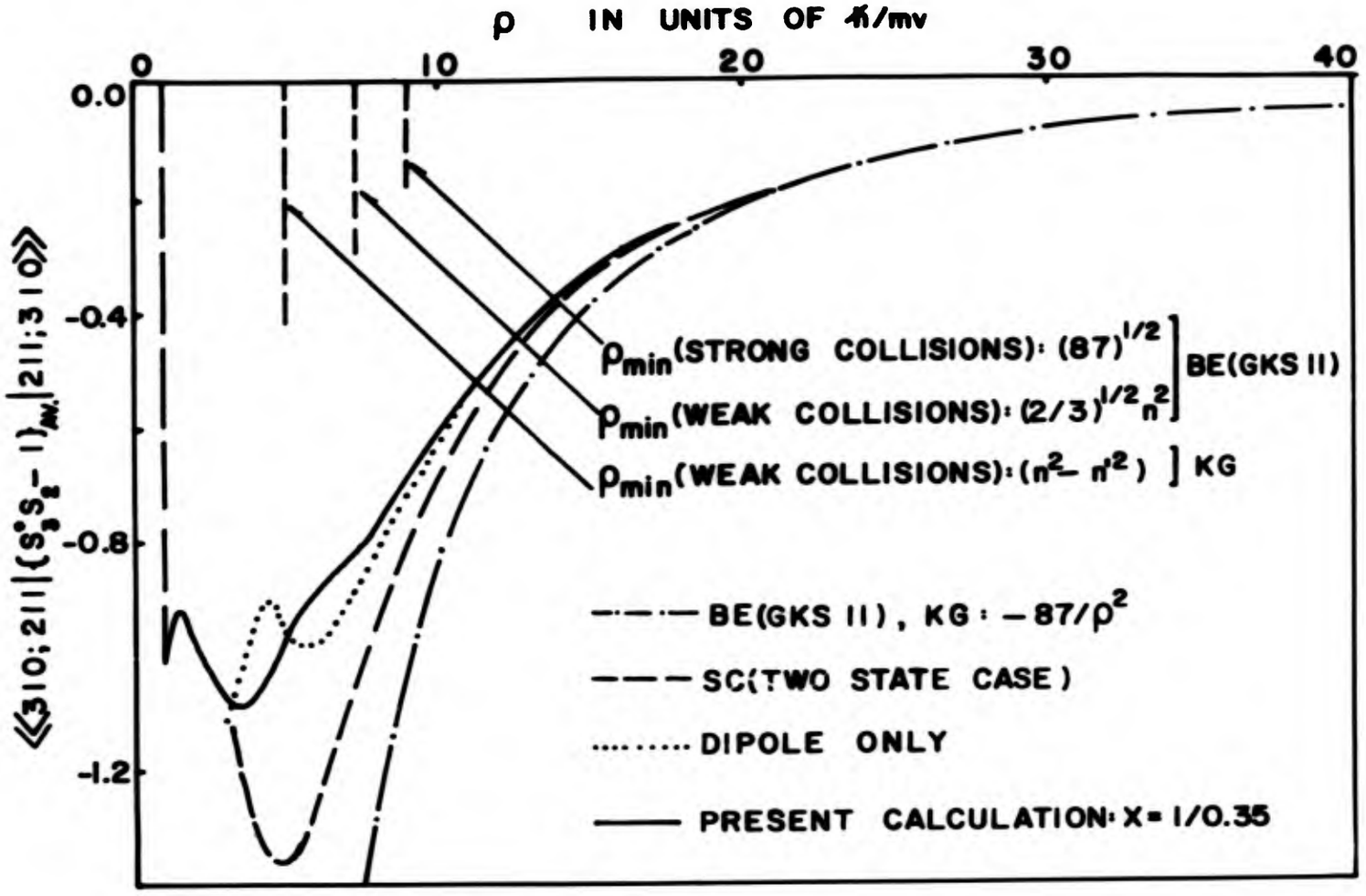

Fig. 5. Typical $\{S_3^* S_2 - 1\}_{av.}$ matrix element as a function of ρ using various approximations. The curves derived in the present calculations are functions of v. The particular curve shown is for v = 0·35 or $X = \hbar/mva_o = 1/0.35$. The BE(GKSII), KG, SC and dipole only curves are independent of v and are shown for comparison. Also shown are the ρ_{min} cut offs used in BE(GKSII) and KG.

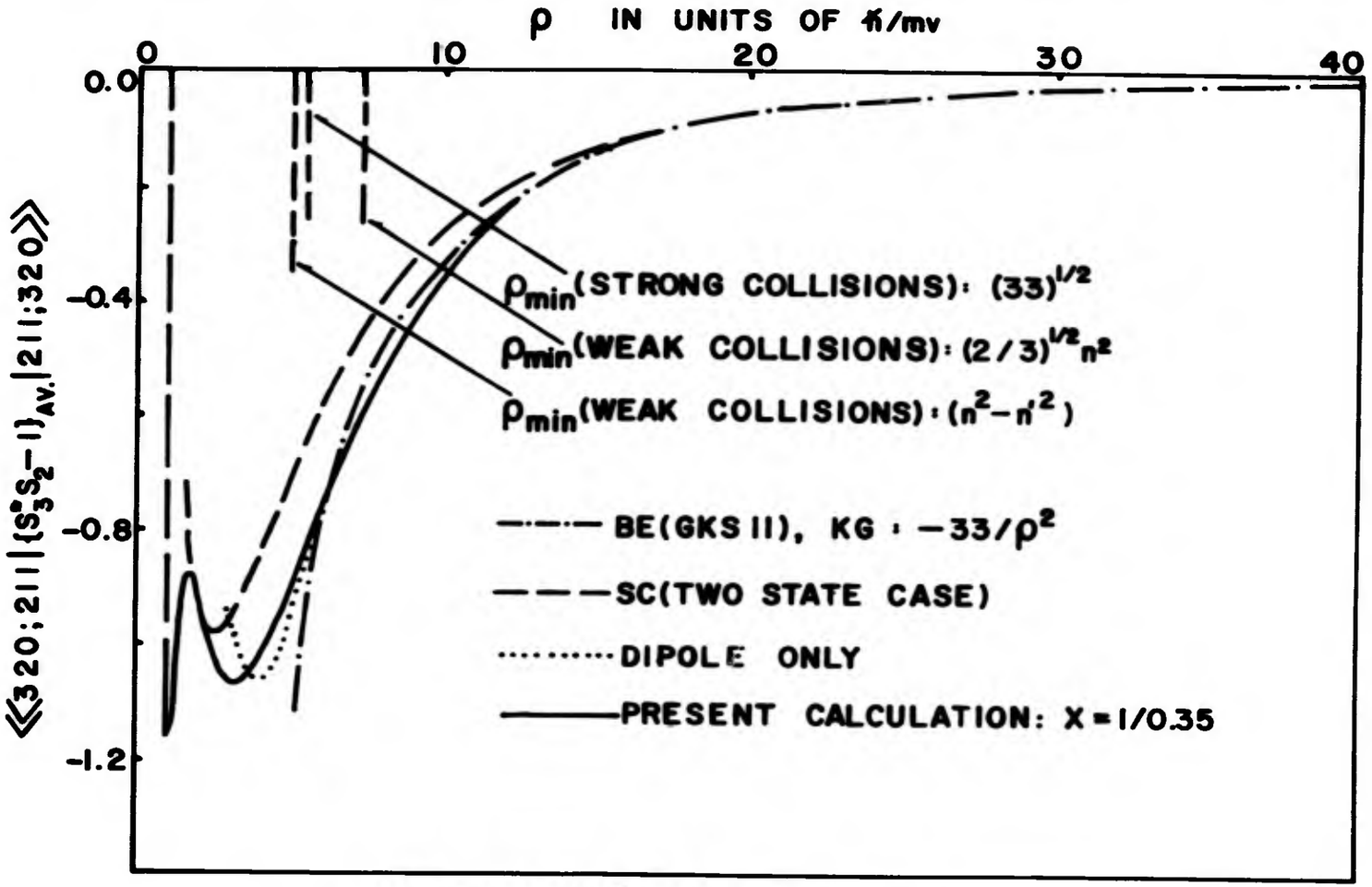

Fig. 6. Typical $(S^{\circ}_3 S_2 - 1)_{av.}$ matrix element as a function of ρ using various approximations. The curves derived in the present calculations are functions of v. The particular curve shown is for v = 0·35 or $X = \hbar/mva_o = 1/0.35$. The BE(GKSII), KG, SC and dipole only curves are independent of v and are shown for comparison. Also shown are the ρ_{min} cut offs used in BE(GKSII) and KG.

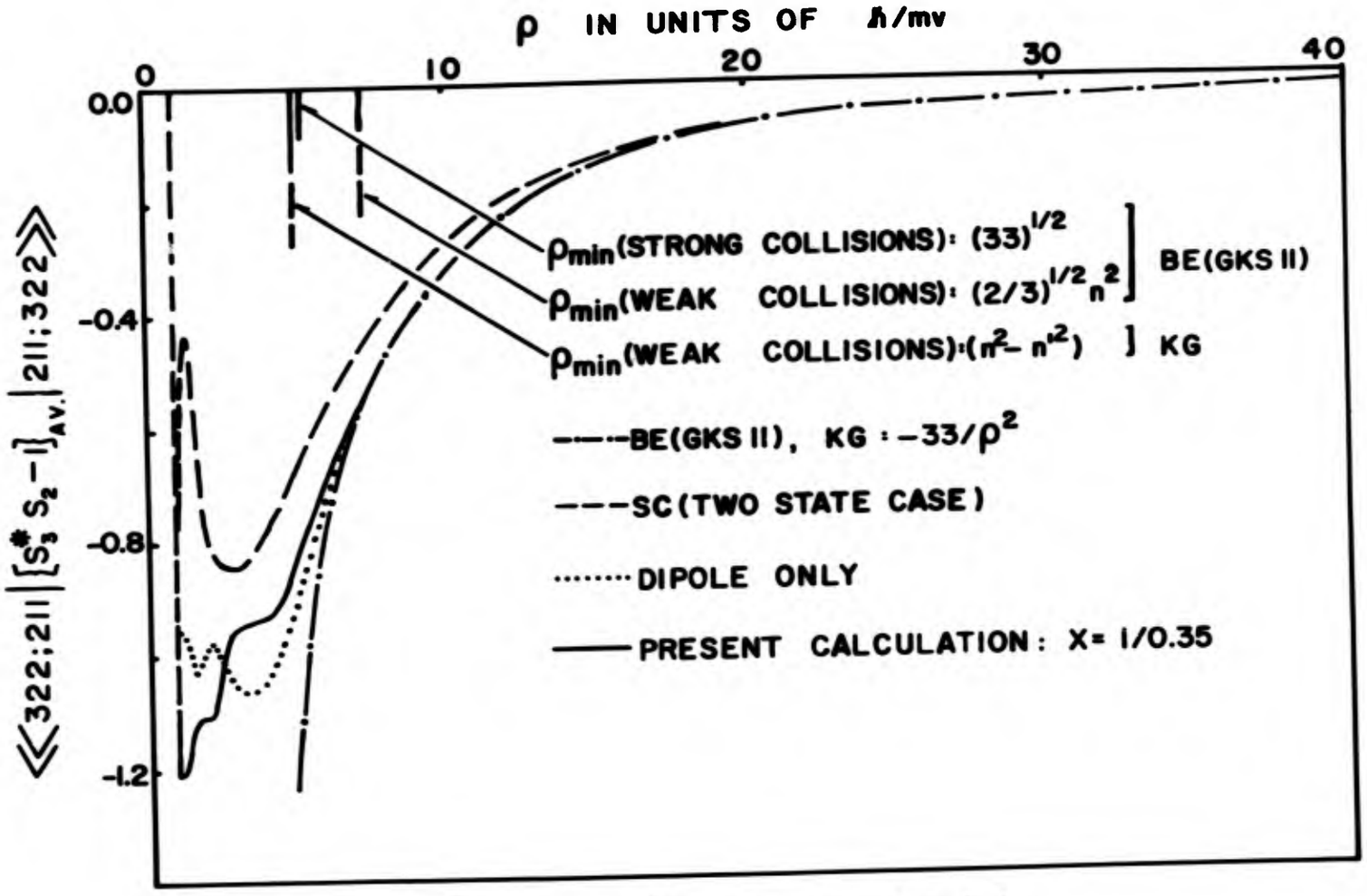

Fig. 7. Typical $\{S_3^* S_2 - 1\}_{av.}$ matrix element as a function of ρ using various approximations. The curves derived in the present calculations are functions of v. The particular curve shown is for v = 0.35 or $X = \hbar/mva_o = 1/0.35$. The BE(GKSII), KG, SC and dipole only curves are independent of v and are shown for comparison. Also shown are the ρ_{min} cut offs used in BE(GKSII) and KG.

the perturber is assumed to be always farther away from the origin than the bound electron, i.e., R > r. This is the same approximation made in performing the SC type calculations. The difference between the "dipole only" and the SC calculations is that the former does not assume that $V(t_1)$ commutes with $V(t_2)$ while the latter does. In other words, comparison of these two curves shows the effects of time ordering. For $\rho < 3\hbar/mv$, the various curves show a good deal of structure and criss-cross at numerous points, making the simultaneous display of the curves in this region impractical. For this reason only the curves for the present calculation are shown for $\hbar \leq \rho \leq 3\hbar/mv$. For $\rho \geq 40\hbar/mv$ the various curves effectively merge into the GKSII curve, indicating that the second order (in V(t)) term of the Dyson expansion is sufficient for treating collisions with large impact parameters as one would expect.

In order to obtain the Φ-matrix elements, the integration over ρ and v (Eq. 4) was performed numerically for ρ, ranging from $\hbar$ to ρ_D (for $\rho > 40\ \hbar/mv$, $\{S_3^* S_2 - 1\}$ av. was set equal to $-(2/3)Q/\rho^2$) and v from 0 to ∞. The lower limit of zero for the velocity should be a good approximation for,

$$(\hbar/m\rho_D)(m/2kT)^{1/2} \ll 1 \qquad (30)$$

(i.e., min. velocity << mean velocity). The resulting Φ matrix elements are conveniently expressed by specifying the K's in Eq. 20 for the various matrix elements. The K's are independent of

TABLE I. Values of K (Eq. 20) determined by the present calculations as a function of temperature. Also shown are the values of K used by KG as a function of temperature. In addition, we show the values of K determined using the formalism of Shen and Cooper as applied to the two-state case. In the GKSI formalism K = 0 while in the GKSII formalism, on which the calculations of BE are based, K = -1. The "dipole only" values are identical to the values given for T = 10^{40}K.

Spherical quantum numbers specifying upper (n) and lower (n') states.						Temperature (^{o}K)					
$n\ell_1 m_1$	$n'\ell_2 m_2$	$n'\ell_4 m_4$	$n\ell_3 m_3$	$2\mathcal{R}/3$(a.u.)	K(SC)	10^4	2×10^4	3×10^4	4×10^4	5×10^4	6×10^4
300	200	200	300	126.0	.132	0.29	0.30	0.33	0.35	0.38	0.40
310	200	200	310	99.0	-.055	0.09	0.11	0.13	0.16	0.18	0.21
311	200	200	311	99.0	-.055	0.09	0.11	0.13	0.16	0.18	0.21
320	200	200	320	45.0	-.676	-0.90	-0.88	-0.85	-0.81	-0.77	-0.73
321	200	200	321	45.0	-.676	-0.90	-0.88	-0.85	-0.81	-0.77	-0.73
300	200	210	310	- 29.4	.983	0.84	0.84	0.85	0.86	0.87	0.89
310	200	210	300	- 29.4	.983	0.70	0.71	0.73	0.75	0.77	0.80
310	200	210	320	- 20.8	.221	0.70	0.70	0.71	0.71	0.72	0.73
311	200	210	321	- 18.0	.221	0.70	0.70	0.71	0.71	0.72	0.73
320	200	210	310	- 20.8	.221	0.54	0.55	0.56	0.57	0.58	0.60
321	200	210	311	- 18.0	.221	0.54	0.55	0.56	0.57	0.58	0.60
311	200	211	300	- 29.4	.983	0.69	0.70	0.72	0.74	0.77	0.79
311	200	211	320	10.4	.221	0.70	0.70	0.71	0.71	0.72	0.73
321	200	211	310	- 18.0	.221	0.54	0.55	0.5[illegible]	0.57	0.58	0.60
300	210	210	300	114.0	.018	0.15	0.18	0.21	0.23	0.26	0.29
310	210	210	310	87.0	-.307	0.09	0.09	0.11	0.12	0.15	0.17
311	210	210	311	87.0	-.346	-0.09	-0.07	-0.04	-0.01	0.02	0.05
320	210	210	320	33.0	-.668	-1.38	-1.35	-1.32	-1.27	-1.22	-1.18
321	210	210	321	33.0	-.724	-1.41	-1.38	-1.35	-1.30	-1.25	-1.20
300	211	211	300	114.0	.018	0.15	0.18	0.21	0.23	0.26	0.29
310	211	211	310	87.0	-.346	-0.09	-0.07	-0.04	-0.01	0.02	0.05
311	211	211	311	87.0	-.327	-0.02	-0.01	0.02	0.04	0.07	0.10
320	211	211	320	33.0	-.836	-1.48	-1.46	-1.42	-1.37	-1.33	-1.28
321	211	211	321	33.0	-.808	-1.38	-1.35	-1.32	-1.27	-1.22	-1.18
322	211	211	322	33.0	-.724	-1.24	-1.22	-1.18	-1.14	-1.09	-1.05
K (KG) = 0.78 + 8kT/3E_H (independent of matrix element)						-0.95	-1.12	-1.29	-1.46	-1.63	-1.80

electron density and are shown as a function of temperature in Table I. Shown for comparison are the KG values which are the same for all elements but depend on temperature. In addition, we show the BE (GKSII) and SC values which are independent of temperature. Not shown are the values based on the "dipole only" calculations since these are identical to the K's given for $T = 10^{4°}K$; i.e., the present calculations approach the "dipole only" calculation as T becomes small (This behavior is similar to that for the case of Lyman-α[5]). The K's shown are seen to be quite different from those based on previous calculations, but the effect on the H_α line profile is difficult to gauge without performing detailed profile calculations.

In order to compute the H_α line profile, the Φ matrix elements (Eq. 20), with the K's given in Table I, were first transformed to the parabolic system using the transformation given in Appendix A. The profile S (α) (Eq. 1) was then calculated in the usual way. In order to compare this with previous calculations, the Φ matrix elements, with the K's based on previous approximations (see Table I), were computed in similar fashion. The resulting profiles for an electron density of 10^{17} e/cm^3 and a temperature of $2 \times 10^{4°}K$ are shown in Fig. 8 (renormalized to a peak intensity of 1). The SC curve lies almost exactly on top of the KG curve

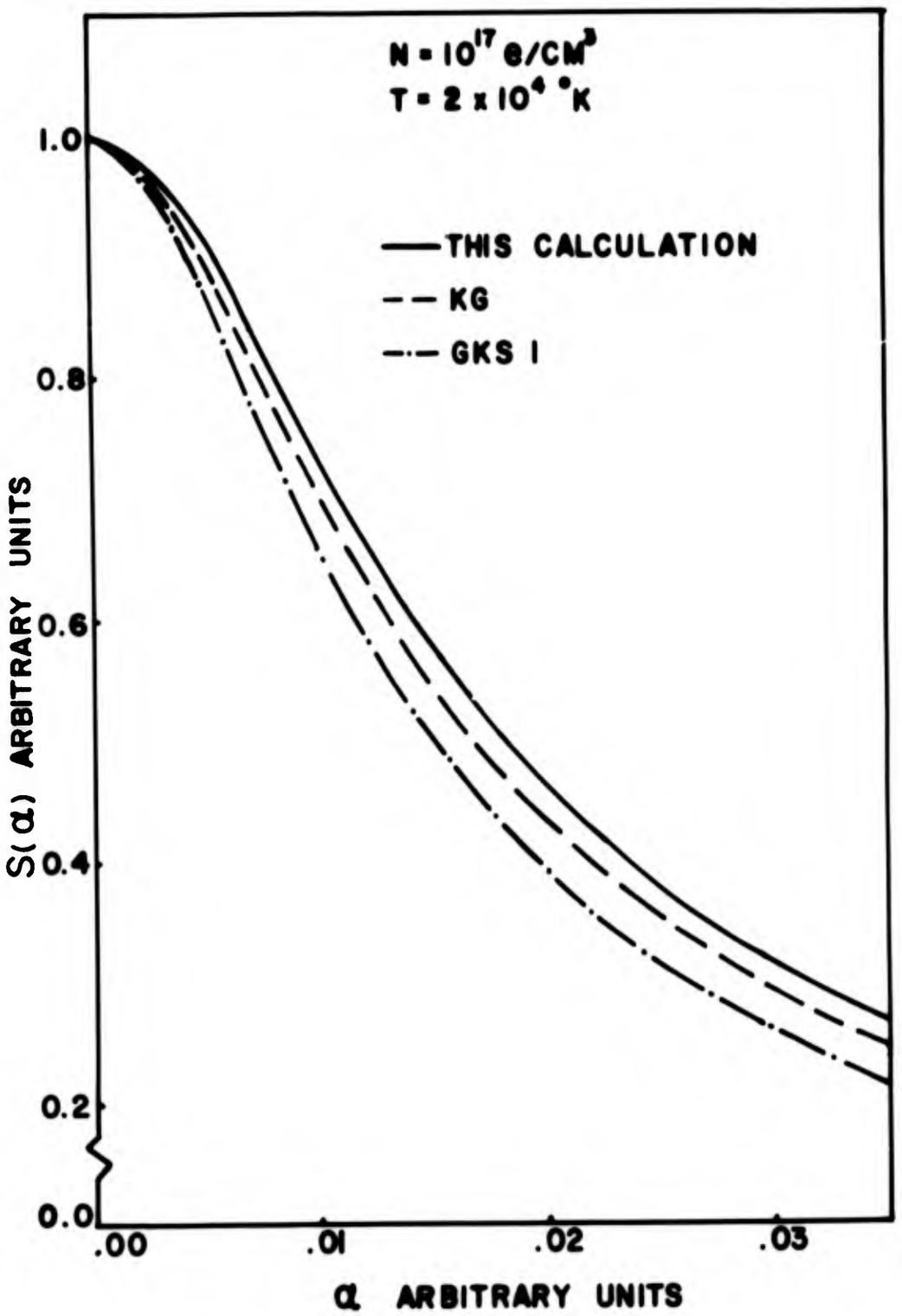

Fig. 8. Comparison of various H_α profiles. The SC and BE curves are not shown. The SC curve lies almost exactly on top of the KG curve and the BE(GKSII) is slightly narrower than the KG curve.

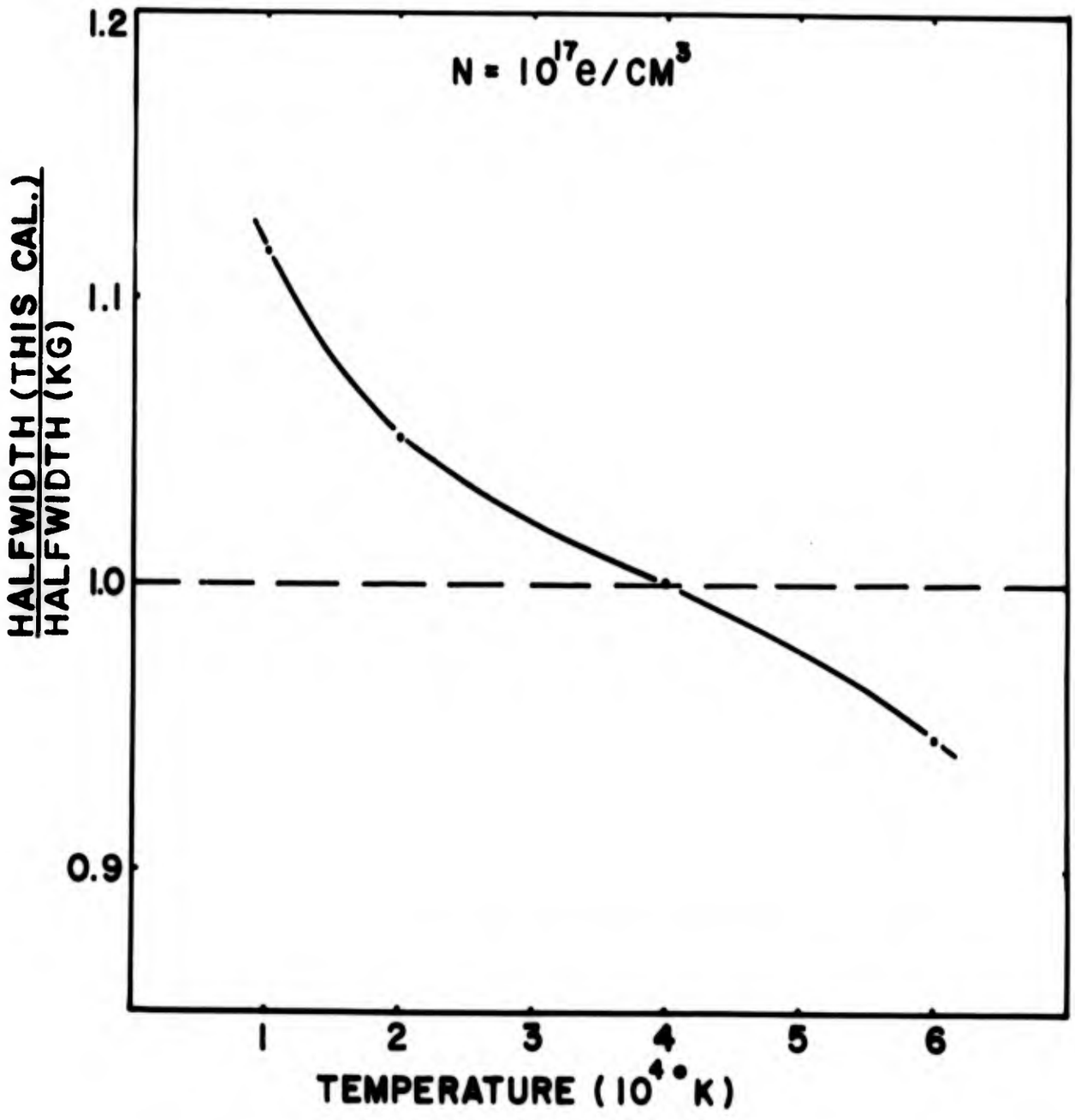

Fig. 9. The ratio of the halfwidths of this calculation to the KG halfwidths as a function of temperature for $N = 10^{17}$ e/cm^3.

and therefore is not shown. The BE (GKSII)* curve is slightly narrower than the KG curve but not sufficiently so as to be distinguishable on the scale used.

In general, profiles based on the present values of K are broader than those based on the K's of the previous approximations. From Fig. 8, the present profile is seen to be $\sim$ 5% broader than the KG profile. This relative comparison is, however, a function of temperature for a given density. This is illustrated in Fig. 9, where we have plotted as a function of temperature the ratio of the halfwidth, using the K's calculated in the present paper to the halfwidth using the K's of KG, for an electron density of 10^{17} e/cm^3. From Fig. 9 we see that the present calculations are $\sim$ 11% broader at $10^{4°}$K and $\sim$ 5% narrower at $6 \times 10^{4°}$K for the particular electron density shown. We note at this point that since KG use the complete $\mathcal{R}$ matrix in their calculations and since the K's determined here are independent of ϕ_{max}, the present calculations should, for a given N and T, show the same relative behavior exhibited in Figs. 8 and 9 if one were to use the upper cut-off procedure of KG. The same cannot be said for the BE calculations of references 2 and 3 since some of the terms of the $\mathcal{R}$ matrix were neglected (see section III) and similarly also for the GKSI calculations.

*The sense in which the curves are characterized has already been mentioned in the introduction.

TABLE II. $\mathcal{G}$ (Eq. 31) as a function of temperature ($T^{\circ}K$)

Spherical quantum numbers specifying upper (n) and lower (n') states				Temperature ($^{\circ}K$)					
$n\ell_1 m_1$	$n'\ell_2 m_2$	$n'\ell_4 m_4$	$n\ell_3 m_3$	10^4	2×10^4	3×10^4	4×10^4	5×10^4	6×10^4
300	200	200	300	-8.77	-12.36	-15.19	-17.66	-19.91	-22.03
310	200	200	310	-5.91	- 8.74	-11.10	-13.20	-15.14	-16.95
311	200	200	311	-5.91	- 8.74	-11.10	-13.20	-15.14	-16.95
320	200	200	320	-2.81	- 4.04	- 5.11	- 6.12	- 7.11	- 8.08
321	200	200	321	-2.81	- 4.04	- 5.11	- 6.12	- 7.11	- 8.08
300	200	210	310	-0.10	- 0.32	- 0.54	- 0.73	- 0.89	- 1.02
310	200	210	300	-0.38	- 0.68	- 0.91	- 1.11	- 1.26	- 1.39
310	200	210	320	-0.23	- 0.34	- 0.44	- 0.52	- 0.59	- 0.65
311	200	210	321	-0.20	- 0.30	- 0.38	- 0.45	- 0.51	- 0.56
320	200	210	310	-0.23	- 0.34	- 0.43	- 0.50	- 0.57	- 0.62
321	200	210	311	-0.20	- 0.30	- 0.37	- 0.43	- 0.49	- 0.54
311	200	211	300	-0.38	- 0.68	- 0.91	- 1.11	- 1.26	- 1.39
311	200	211	320	0.12	0.17	0.22	0.26	0.29	0.32
321	200	211	310	-0.20	- 0.30	- 0.37	- 0.43	- 0.49	- 0.54
300	210	210	300	-9.28	-13.35	-16.62	-19.49	-22.11	-24.55
310	210	210	310	-7.54	-10.97	-13.78	-16.26	-18.51	-20.61
311	210	210	311	-6.87	-10.21	-12.99	-15.47	-17.74	-19.85
320	210	210	320	-4.19	- 6.01	- 7.52	- 8.91	-10.21	-11.48
321	210	210	321	-4.17	- 5.96	- 7.46	- 8.83	-10.12	-11.38
300	211	211	300	-9.28	-13.35	-16.62	-19.49	-22.11	-24.55
310	211	211	310	-6.88	-10.22	-13.00	-15.48	-17.75	-19.86
311	211	211	311	-7.25	-10.69	-13.53	-16.04	-18.32	-20.44
320	211	211	320	-4.14	- 5.88	- 7.34	- 8.67	- 9.94	-11.18
321	211	211	321	-4.04	- 5.82	- 7.31	- 8.68	- 9.98	-11.24
322	211	211	322	-3.96	- 5.79	- 7.35	- 8.77	-10.12	-11.41

Up to this point, we have considered only the real part of the Φ matrix elements. In addition to the real part, the Φ matrix elements have an imaginary part which tends to zero as the real part approaches the GKSII curves (Figs. 4-7); i.e., $\rho \gtrsim 40\ \hbar$/mv. The integration over ρ and v of the imaginary part of $\{S_3^* S_2 - 1\}$ av. was performed in much the same way as the integration of the real part. In Table II we have tabulated the quantity $\mathcal{J}$ for the relevant matrix elements as a function of temperature where,

$$\mathrm{Im}\,\Phi = C\,\mathcal{J} \tag{31}$$

C is given by Eq. 16. Including the imaginary part of the Φ matrix elements in the H_α profile calculations results in a shift to the red with no apparent assymetry about the peak intensity. At $2 \times 10^{4^\circ}$K and a density of 10^{17} e/cm^3, the red shift ~ 0.3Å while at the same temperature; but at a density of 10^{18} e/cm^3, the shift is ~ 1.9Å.

V DISCUSSION AND CONCLUSION

Using the straight line classical path model, we have calculated the impact broadening operator Φ for the hydrogen line H_α (6563Å). By performing the calculations numerically, we have preserved the correct time ordering and included all contributing orders in the multipole interaction; i.e., we have included multipoles up to and including 2(n-1) for n = 2 and n = 3. A comparison between the present and previous Φ matrix elements is made in terms of the constants K in analogy to the Lyman-α case considered in reference 5. The numerical values of the K's are estimated to be accurate to $\pm$ 0.05. The K's are found to differ quite appreciably from previous estimates and to exhibit a behavior similar to that of the K's obtained in the case of Lyman-α; i.e., both positive and negative K's are found (note the difference in the sign convention used here and that used for the Lyman-α case). The negative K's decrease in absolute magnitude as the temperature increases, while the positive K's increase. Previous estimates of K are independent of temperature except the K's of KG which vary in the opposite sense with temperature compared to the present K's.

In order to demonstrate the effect of the K's on the H_α line profile, typical profiles were calculated using the present K's. These were then compared with the H_α profile using the K's based on previous approximations. In order to do this, the maximum impact parameter was set equal to the Debye length ρ_D and the complete $\mathcal{R}$ matrix was retained. By this procedure, a relative

comparison was made which reflects the treatment of collisions with small impact parameters used in the various calculations rather than the calculations themselves. However, since KG use the complete Q matrix and the K's are independent of ρ_{max}, the relative comparison of the halfwidths indicated in Fig. 9 should also remain valid in an absolute sense; i.e., the ratio of the present halfwidths to those characterized as KG should remain the same if one were to use the cut-off procedure of KG rather than the $\rho_{max} = \rho_D$ used here. We note that this does not apply to the calculations characterized as GKSI and BE(GKSII) in this report.

It is interesting to note that the present halfwidths deviate from those of KG for T between $10^{4°}$K and $2 \times 10^{4°}$K by approximately the same amount as the BE(GKSII) halfwidths deviate from the KG halfwidths and would perhaps indicate why the BE(GKSII) results appear to agree "better" than those of KG with some of the experimental results.[25, 11, 14] However, it may be that in the final analysis, deviation from the KG values using the present values of K may be quite different if a ρ_{max} of $0.682\rho_D$, as suggested by Chappell, et.al.[16], is used for the upper cut-off instead of the ρ_D used here.

Inclusion of the imaginary part of the Φ matrix elements results in a slight shift to the red with no discernible assymetry about the peak. The shift depends primarily on electron density and to a lesser degree on temperature. For the two examples

chosen in this report, the shift is 0.3Å and 1.9Å for T = 2×10^{4}°K and N = 10^{17} e/cm^3, and T = 2×10^{4}°K and N = 10^{18} e/cm^3 respectively.

In conclusion it should be pointed out that even though the use of the classical path approximation below the ρ_{min} cut offs of previous calculations is somewhat questionable and quantum effects are possibly significant the present calculations should be a definite improvement over the almost arbitrary treatment of strong collisions used in previous calculations.

Apart from possible quantum effects for small ρ there remain, questions regarding (1) correlations which determine the upper cut off ρ_{max} (2) the significance of the breakdown of the quasi static treatment for the ions at the line center. In addition causes of assymetry should be included in the computations. Remaining discrepancies could then be ascribed to (1) breakdown of the Classical path approximation (2) the neglect of terms involving a sum over states with different principal number on the R.H.S. of Eq. 6, for collisions with small ρ, and not to arbitrary variations in ρ_{min} and arbitrary strong collision corrections as would be possible heretofore.

VI REFERENCES

1. Anderson, P. W., Phys. Rev. 76, 647 (1949)

2. Bacon, M. E., and Edwards, D. F., Phys. Rev. 170, 125 (1968)

3. Bacon, M. E., and Edwards, D. F., ARL Report # 69-0109 (1969)

4. Bacon, M. E., and Edwards, D. F., J. Quant. Spec. Rad. Trans. 10, 503 (1970)

5. Bacon, M. E., Shen, K. Y., and Cooper, J., Phys. Rev. 188, 50 (1969)

6. Baranger, M., Phys. Rev. 111, 494 (1958)

   Baranger, M., Phys. Rev. 111, 481 (1958)

   Baranger, M., Phys. Rev. 112, 855 (1958)

7. Baranger, M., in "Atomic and Molecular Processes", ed. Bates, D. R. (New York: Academic Press, 1962)

8. Ben Reuven, A., Phys. Rev. 141, 34 (1966)

   Ben Reuven, A., Phys. Rev. 145, 7 (1966)

   Fano, U., Phys. Rev. 131, 259 (1963)

   Zaidi, H. R., Phys. Rev. 173, 132 (1968)

   Ross, D. W., An. Phys. (N.Y.), 36, 458 (1966)

   Klien, L., J. Quant. Spec. Rad. Trans. 9, 199 (1969)

   Bezzerides, B., J. Quant. Spec. Rad. Trans. 7, 353 (1967)

   Bezzerides, B., Phys. Rev. 159, 3 (1967)

   Cooper, J., Rev. Mod. Phys. 39, 167 (1967)

   Davis, J., Proc. Phys. Soc. 90, 283 (1967)

   Smith, E. W., and Hooper, Jr. , C. F., Phys. Rev. 157, 126 (1967)

   Smith, E. W., Phys. Rev. 166, 102 (1968)

9. Berg, H. F., Ali, A. W., Lincke, R., and Griem, H. R., Phys. Rev. 125, 199 (1962)

10. Bethe, H. A., and Salpeter, E. E., "Quantum Mechanics of One and Two-Electron Atoms", (Berlin: Springer Verlag, 1957)

11. Birkeland, J. W., Oss, J. P., and Braun, W. G., Phys. Rev. 178, 368 (1969)

12. Birkeland, J. W., and Oss, J. P., Appl. Opt. 4, 589 (1968)

13. Braun, W. G., Rev. Sci. Instr. 36, 802 (1965)

14. Bridges, J. M., and W. L. Wiese, in Proceedings of the 7th International Conference on Phenomena in Ionized Gases (Gradevinska Knjiga Publishing House, Belgrade, 1966), Vol. II, p. 165

15. Cooper, J. Rev. Mod. Phys. 39, 167 (1967)

16. Chappell, W., Cooper, J., and Smith, E. W., J. Quant. Spec. Rad. Trans. 9, 149 (1969)

17. Ecker, G., Z. Physik 148, 593 (1957)

18. Edmonds, A. R., "Angular Momentum in Quantum Mechanics" (Princeton, New Jersey: Princeton University Press, 1957)

19. Griem, H. R., Kolb, A. C., and Shen, K. Y., Phys. Rev. 116, 4 (1959)

20. Griem, H. R., Phys. Rev. 140, A1140 (1965); also Errata Phys. Rev. 144, 366 (1966)

21. Griem, H. R., "Plasma Spectroscopy" (New York: McGraw-Hill Book Co., 1964)

22. Griem, H. R., Kolb, A. C., and Shen, K. Y., Astrophys. J. 135, 272 (1962)

23. Griem, H. R., Astrophys. J. 148, 547 (1967)

24. Griem, H. R., Baranger, M., Kolb, A. C., and Oertel, G., Phys. Rev. 125, 177 (1962)

25. Griffith, R., Bober, L., and Tankin, R. S., Plasma Physics 11, 529 (1969)

26. Hooper, Jr., C. F., Phys. Rev. 165, 215 (1968)

27. Hughes, J. W. B., Proc. Phys. Soc. 91, 810 (1967)

28. Kepple, P., and Griem, H. R., Phys. Rev. 173, 317 (1968)

29. Kolb, A. C., and Griem, H. R., Phys. Rev. 111, 514 (1958)

30. Minaeva, A. A., Soviet Astronomy-AJ, 12, 495 (1968)

31. Mozer, B., and Baranger, M., Phys. Rev. 118, 626 (1960)

32. Popenoe, C. H., and Shumaker, Jr., J. B., J. Res. NBS 69A, 495 (1965)

33. Rose, M. E., "Elementary Theory of Angular Momentum" (New York: John Wiley, 1957)

34. Shen, K. Y., and Cooper, J., Astrophys. J. 155, 37 (1969)

35. Smith, E. W., Vidal, C. R., and Cooper, J., J. Res. NBS, 73 , 389 (1969)

Smith, E. W., Vidal, C. R., and Cooper, J., J. Res. NBS, 73 , 405 (1969)

36. Underhill, A. B., and Waddell, J., NBS Circular 603 (Washington, D. C.: U. S. Government Printing Office, 1959)

37. Wiese, W. L., "Plasma Diagnostic Techniques," ed. Huddlestone, R. H., and Leonard, S. L. (New York: Academic Press), Chap. 6 (1965)

APPENDIX A

Transformation from Spherical to Parabolic Coordinates

In the one state case we require the transformation $\langle n_1 n_2 m | n \ell m' \rangle$. This transformation has been determined by Hughes[27] in terms of the angular momentum Clebsch-Gordon coefficients as defined by Rose[33]. In this report we use the notation of Edmonds[18] in terms of which the transformation may be written:

$$\langle n_1 n_2 m | n \ell m' \rangle = \delta_{mm'} (-1)^{n_2 + (|m|+m)/2} (2\ell+1)^{1/2} \begin{pmatrix} \tfrac{1}{2}(n-1) & , \tfrac{1}{2}(n-1) & , \ell \\ \tfrac{1}{2}(m+n_2-n_1), & \tfrac{1}{2}(m+n_1-n_2), & -m \end{pmatrix}$$

The transformation in the two state case is simply a product of 2 such terms. We shall use a notation consistent with the "doubled atom" notation of Baranger[6]. The "doubled transformation" is then given by,

$$\ll n_1 n_2 m; n_1' n_2' m' | n \ell m''; n' \ell' m'' \gg = \delta_{mm''} \delta_{m'm'''} (2\ell+1)^{1/2} (2\ell'+1)^{1/2} (-1)^{n_2 + n_2' + (|m|+m)/2 + (|m'|+m')/2}$$

$$\times \begin{pmatrix} \tfrac{1}{2}(n-1) & , \tfrac{1}{2}(n-1) & \ell \\ \tfrac{1}{2}(m+n_2-n_1), & \tfrac{1}{2}(m+n_1-n_2), & -m \end{pmatrix} \begin{pmatrix} \tfrac{1}{2}(n'-1) & , \tfrac{1}{2}(n-1) & , \ell' \\ \tfrac{1}{2}(m'+n_2'-n_1'), & \tfrac{1}{2}(m'+n_1'-n_2'), & -m' \end{pmatrix}$$

In the case of H_α the line space and therefore the "doubled transformation" has dimension $(2^2 \times 3^2) = 36$. Due to the symmetry[6] we need consider only the reduced line space (see reference 3) which has dimension 16. The reduced doubled transformation relevant to the H_α line is shown in Fig. (AI). In Table AI and AII we give for completeness the single trans-

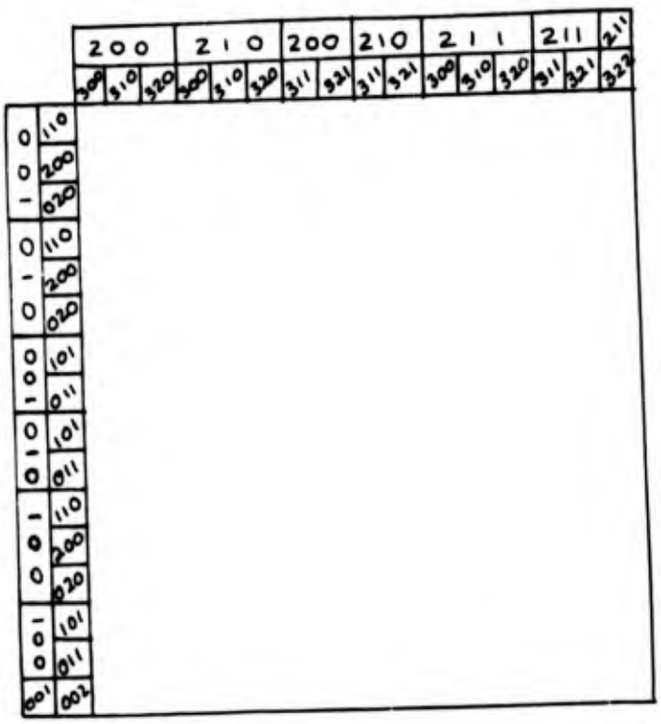

Fig A1. The reduced doubled transformation $\ll n_1 n_2 m; n'_1 n'_2 m' \mid n \ell m''; n' \ell' m'' \gg$ for the H_α line of Hydrogen.

Table AI

Transformation from Spherical to Parabolic Wave Functions for the $n' = 2$ levels

n_1	n_2	m	n	ℓ	m	$\langle n_1 n_2 m \mid n \ell m \rangle$
0	0	1	2	1	1	1
0	1	0	2	0	0	$-1/\sqrt{2}$
0	1	0	2	1	0	$-1/\sqrt{2}$
1	0	0	2	0	0	$-1/\sqrt{2}$
1	0	0	2	1	0	$1/\sqrt{2}$
0	0	1	2	1	-1	-1

Table AII

Transformation from Spherical to Parabolic Wave Functions for the n = 3 Levels

n_1	n_2	m	n	ℓ	m	$\langle n_1 n_2 m \mid n\ell m \rangle$
0	0	2	3	2	2	1
0	1	1	3	1	1	$-1/\sqrt{2}$
0	1	1	3	2	1	$-1/\sqrt{2}$
1	0	1	3	1	1	$-1/\sqrt{2}$
1	0	1	3	2	1	$1/\sqrt{2}$
0	2	0	3	0	0	$1/\sqrt{3}$
0	2	0	3	1	0	$1/\sqrt{2}$
0	2	0	3	2	0	$1/\sqrt{6}$
1	1	0	3	0	0	$1/\sqrt{3}$
1	1	0	3	2	0	$-1\sqrt{2}/3$
2	0	0	3	0	0	$1/\sqrt{3}$
2	0	0	3	1	0	$-1/\sqrt{2}$
2	0	0	3	2	0	$1/\sqrt{6}$
0	1	-1	3	1	-1	$1/\sqrt{2}$
0	1	-1	3	2	-1	$1/\sqrt{2}$
1	0	-1	3	1	-1	$1/\sqrt{2}$
1	0	-1	3	2	-1	$-1/\sqrt{2}$
0	0	-2	3	2	-2	1

formation for the $n' = 2$ and $n = 3$ levels respectively. The reduced doubled transformation of Fig. AI may be derived from these transformation elements.

APPENDIX B

The first part of this appendix, including the V (t) matrix elements for the n' = 2 levels, is essentially the same as the appendix of Ref. 5 and is included here for completeness.

The coordinate system in which the straight-line-classical path interaction (V(t)) of a free electron and radiating atom is to be evaluated is shown in Fig. B1. This set of axes is what Anderson[1] has called the collision axes and are chosen as a matter of convenience. The z-axis is chosen to lie along the direction of $\vec{v}$ and the x-axis to lie along the direction $\vec{v}$. The zero of time is taken to be the time of closest approach. The origin of the coordinate system is located at the center of mass of the atomic system, which, for all practical purposes, is at the nucleus. The atomic electron is located at (r,θ', φ') and the free electron at (R, θ, 0). Denoting the angle between $\vec{R}$ and $\vec{r}$ by β' we may write the interaction energy as,

$$V(R) = \begin{cases} (1/r - 1/R) + \sum_{i=1}^{\infty} (R^i/r^{i+1}) P_i(\cos\beta') & r > R \\ \sum_{i=1}^{\infty} (r^i/R^{i+1}) P_i(\cos\beta') & r < R \end{cases} \qquad \text{(B1)}$$

The first term in the upper expression is the monopole contribution; and the index i in the summation specifies the 2^i- pole contribution.

Using the addition theorem for spherical harmonics (the definitions given by Edmonds[18] are used throughout), the i-th

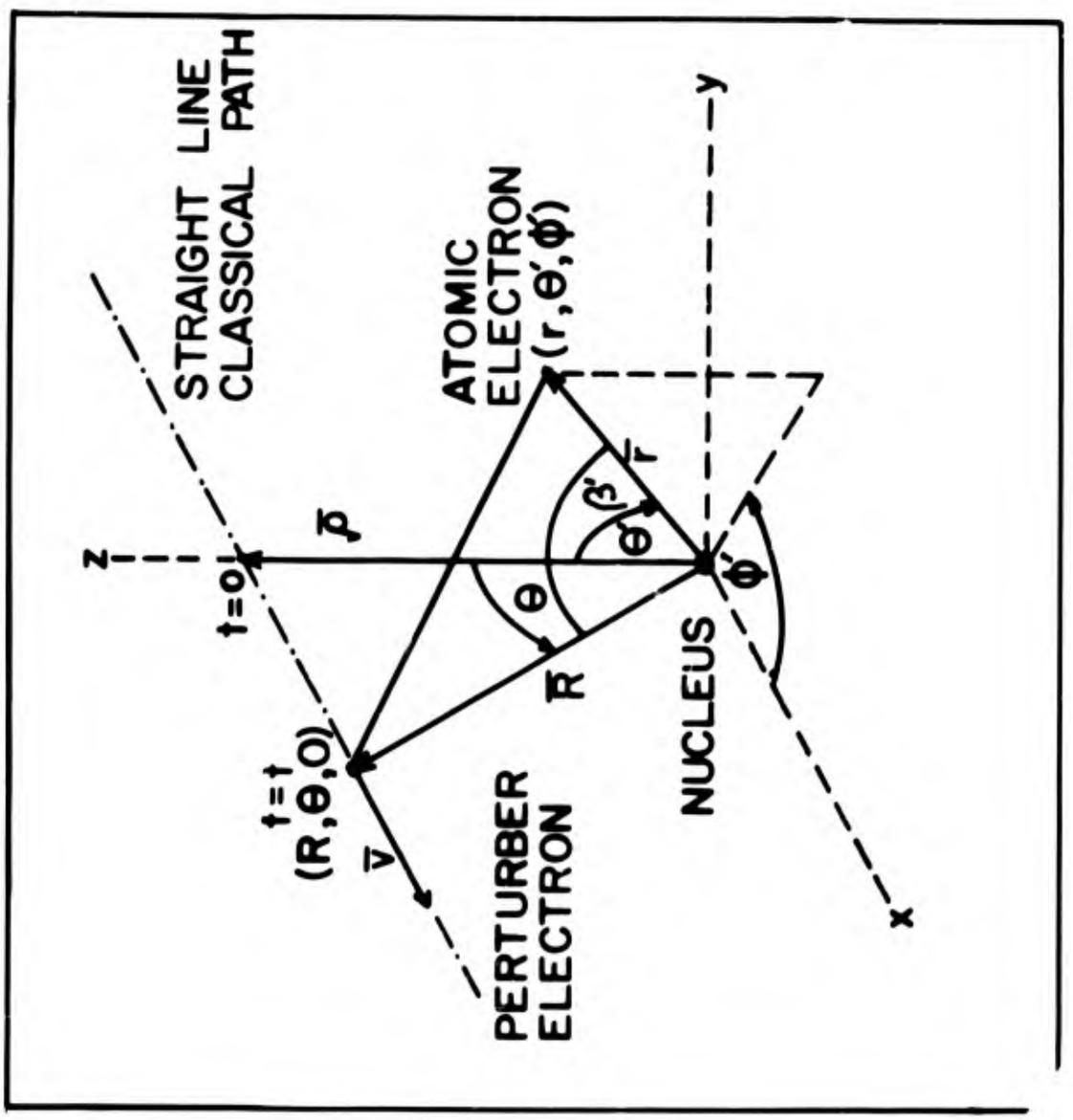

Fig. B1. Collision Axes.

term in the interaction energy ($i \neq 0$) may be written,

$$V^i(R) = 4\pi(2i+1)^{-1}\sum_{m=-i}^{i} Y^*_{im}(\theta'\phi')Y_{im}(\theta\phi)\begin{cases} R^i/r^{i+1} & r>R \\ r^i/R^{i+1} & r<R \end{cases} \quad \text{(B2)}$$

The $i = 0$ term remains as in Eq. B1. The angular average can best be performed when the $|n\ell m\rangle$ wave functions are used as bases (see Cooper[15]). For this reason we chose to evaluate Eq. (9), Section II in terms of the $|n\ell m\rangle$ states. In evaluating Eq. (9) we require the matrix elements $\langle n\ell m|V^i|n\ell' m'\rangle$. Using Eq. (B2) we obtain,

$$\langle n\ell m|V^i(R)|n\ell' m'\rangle = \left[\int_0^R R^*_{n\ell}\frac{r^i}{R^{i+1}}R_{n\ell'}dr + \int_R^\infty R^*_{n\ell}\frac{R^i}{r^{i+1}}R_{n\ell'}dr\right]$$
$$\times 4\pi(2i+1)^{-1}\int_0^{2\pi}\sin\theta'd\theta'\int_0^{\pi}Y^*_{\ell m}(\theta'\phi')Y_{\ell' m'}(\theta'\phi')\sum_{m=-i}^{i}Y^*_{im}(\theta'\phi')Y_{im}(\theta\phi)d\phi' \quad \text{(B3)}$$

The angular part of this expression consists of a sum of terms of the form,

$$\left\{\int_0^{2\pi}\sin\theta'd\theta'\int_0^{\pi}Y_{\ell_1 m_1}(\theta'\phi')Y_{\ell_2 m_2}(\theta'\phi')Y_{\ell_3 m_3}(\theta'\phi')\,d\phi'\right.$$
$$= \left[\frac{(2\ell_1+1)(2\ell_2+1)(2\ell_3+1)}{4\pi}\right]^{1/2}\begin{pmatrix}\ell_1 & \ell_2 & \ell_3\\ 0 & 0 & 0\end{pmatrix}\begin{pmatrix}\ell_1 & \ell_2 & \ell_3\\ m_1 & m_2 & m_3\end{pmatrix} \quad \text{(B4)}$$

multiplied by $(-1)^{m_3+m_1}\,Y_{\ell_3-m_3}(\theta\phi)$.

From the properties of the 3-j symbols (last 2 terms in Eq. (B4) the l's and m's must satisfy the conditions

$$\vec{\ell}_1+\vec{\ell}_2=\vec{\ell}_3,$$
$$\ell_1+\ell_2+\ell_3 \quad \text{even},$$
$$m_1+m_2=-m_3,$$
$$\text{and } |m_1|\leq\ell_1,\ |m_2|\leq\ell_2,\ |m_3|\leq\ell_3$$

TABLE BI. V(t) matrix elements for the n = 2 levels

n	ℓ_2	m_2	n	ℓ_4	m_4	2^0-pole	2^1-pole	2^2-pole
2	0	0	2	0	0	$-e^{-R}(8/R+6+2R+R^2)/8$		
2	0	0	2	1	-1		$vtF(R)/\sqrt{6}\ R$	
2	0	0	2	1	0		$\rho F(R)/\sqrt{3}\ R$	
2	0	0	2	1	1		$-vtF(R)/\sqrt{6}\ R$	
2	1	-1	2	1	-1	$-e^{-R}(4/R+3+R+R^2/6)/4$		$(v^2t^2-2\rho^2)G(R)/10R^2$
2	1	-1	2	1	0			$3/\sqrt{2}\ vt\rho G(R)/10R^2$
2	1	-1	2	1	1			
2	1	0	2	1	0	$-e^{-R}(4/R+3+R+R^2/6)/4$		$(2\rho^2-v^2t^2)G(R)/5R^2$
2	1	0	2	1	1			$-3/\sqrt{2}\ vt\rho G(R)/10R^2$
2	1	1	2	1	1	$-e^{-R}(4/R+3+R+R^2/6)/4$		$(v^2t^2-2\rho^2)G(R)/10R^2$

$$F(R) = -9(1-e^{-R}\sum_{n=0}^{4} R^n/n!)/\sqrt{3}R^2$$

$$G(R) = 30(1-e^{-R}\sum_{n=0}^{5} R^n/n!)/R^3+R^2e^{-R}/24$$

$$R = |\vec{\rho} + \vec{v}t|$$

TABLE BII. Angular dependence of the V(t) matrix elements for the n = 3 levels: $a = \sin\theta$, $b = \cos\theta$

ni_1m_1	ni_3m_3	2^0-pole	2^1-pole	2^2-pole	2^3-pole	2^4-pole
300	300	1				
300	310		$(1/\sqrt{3})b$			
300	311		$(-1/\sqrt{6})a$			
300	31-1		$(1/\sqrt{6})a$			
300	320			$(1/\sqrt{20})(2b^2-a^2)$		
300	321			$-\sqrt{3/10}\ ab$		
300	32-1			$\sqrt{3/10}\ ab$		
300	322			$\sqrt{3/40}\ a^2$		
300	32-2			$\sqrt{3/40}\ a^2$		
310	310	1		$(1/5)(2b^2-a^2)$		
310	311			$(-3/5)\sqrt{1/2}\ ab$		
310	31-1			$(3/5)\sqrt{1/2}\ ab$		
310	320		$(2/\sqrt{15})b$		$(1/7)\sqrt{27/20}\ (2b^3-3a^2b)$	
310	321		$(-1/\sqrt{10})a$		$(-3/14)\sqrt{2/5}\ (4b^2a-a^3)$	
310	32-1		$(1/\sqrt{10})a$		$(3/14)\sqrt{2/5}\ (4b^2a-a^3)$	
310	322				$(1/14)\sqrt{45/2}\ ba^2$	
310	32-2				$(1/14)\sqrt{45/2}\ ba^2$	
311	311	1		$(-1/10)(2b^2-a^2)$		
311	31-1			$(-3/10)a^2$		
311	320		$(1/\sqrt{30})a$		$(-3/14)\sqrt{3/10}(4b^2a-a^3)$	
311	321		$(1/\sqrt{5})b$		$(-3/7)\sqrt{1/20}\ (2b^3-3a^2b)$	
311	32-1				$(-1/14)\sqrt{45}\ ba^2$	
311	322		$(-1/\sqrt{5})a$		$(3/28)\sqrt{1/5}\ (4b^2a-a^3)$	
311	32-2				$(-3/28)\sqrt{5}\ a^3$	

TABLE BII. (Continued)

$n\ell_1 m_1$	$n\ell_3 m_3$	2^0-pole	2^1-pole	2^2-pole	2^3-pole	2^4-pole
31-1	31-1	1		$(-1/10)(2b^2-a^2)$		
31-1	320		$(1/\sqrt{30})a$		$(3/14)\sqrt{3/10}\,(4b^2a-a^3)$	
31-1	321				$(-3/14)\sqrt{5}\,ba^2$	
31-1	32-1		$(1/\sqrt{5})b$		$(-3/14)\sqrt{1/5}\,(2b^3-3ba^2)$	
31-1	322				$(3/28)\sqrt{5}\,a^3$	
31-1	32-2		$(1/\sqrt{5})b$		$(-3/28)\sqrt{1/5}\,(4b^2a-a^3)$	
320	320	1		$(1/7)(2b^2-a^2)$		$(2/7)(35/8b^4-15/4b^2+3/8)$
320	321			$(-1/7)\sqrt{3/2}\,ba$		$(-5/28)\sqrt{2/3}\,(7b^3-3b)a$
320	32-1			$(1/7)\sqrt{3/2}\,ba$		$(5/28)\sqrt{2/3}\,(7b^3-3b)a$
320	322			$(-1/7)\sqrt{3/2}\,a^2$		$(5/84)\sqrt{2/3}\,a^2(7b^2-1)$
320	32-2			$(-1/7)\sqrt{3/2}\,a^2$		$(5/84)\sqrt{2/3}\,a^2(7b^2-1)$
321	321	1		$(1/14)(2b^2-a^2)$		$(-4/21)(35/8b^4-15/4b^2+3/8)$
321	32-1			$(-3/14)a^2$		$(-5/42)(7b^2-1)a^2$
321	322			$(-3/7)ab$		$(5/84)(7b^3-3b)a$
321	32-2					$(-5/12)a^3b$
32-1	32-1	1		$(1/14)(2b^2-a^2)$		$(-4/21)(35/8b^4-15/4b^2+3/8)$
32-1	322					$(5/12)a^3b$
32-1	32-2			$(3/7)ab$		$(-5/84)(7b^3-3b)a$
322	322	1		$(-1/7)(2b^2-a^2)$		$(1/21)(35/8b^4-15/4b^2+3/8)$
322	32-2					$(5/24)a^4$
32-2	32-2	1		$(-1/7)(2b^2-a^2)$		$(1/21)(35/8b^4-15/4b^2+3/8)$

in order for non zero terms to exist. These conditions limit the number of non-zero terms in the interaction energy to a finite number. For a particular set of levels with principal quantum number n, $i \leq 2(n-1)$.

For the $n' = 2$ level only terms up to and including the quadrupole terms contribute. The V(t) matrix is symmetric and the relevant non-zero terms for the $n' = 2$ level using Eq. B3 are given in Table B1.

In the case of the n = 3 levels we require terms up to and including the 2^4-pole term. The angular part of the V(t) matrix elements are given in Table BII, while in Table BIII are given the asymtotic values of the radial integrals. For R small the radial integrals were computed numerically using an algorithm supplied by Mr. Raymond of the computer center. The V(t) matrix is again symmetric and hence only the diagonal and half off diagonal elements are listed in Tables BII and BIII.

TABLE BIII. (Continued)

$n\ell_1 m_1$	$n\ell_3 m_3$	2^0-pole	2^1-pole	2^2-pole	2^3-pole	2^4-pole
31-1	31-1			$180.0/R^3$		
31-1	320		$-10.06/R^2$		$-2112.0/R^4$	
31-1	321				$-2112.0/R^4$	
31-1	32-1		$-10.06/R^2$		$-2112.0/R^4$	
31-1	322				$-2112.0/R^4$	
31-1	32-2		$-10.06/R^2$		$-2112.0/R^4$	
320	320			$126.0/R^3$		$25500/R^5$
320	321			$126.0/R^3$		$25500/R^5$
320	32-1			$126.0/R^3$		$25500/R^5$
320	322			$126.0/R^3$		$25500/R^5$
320	32-2			$126.0/R^3$		$25500/R^5$
321	321			$126.0/R^3$		$25500/R^5$
321	32-1			$126.0/R^3$		$25500/R^5$
321	322			$126.0/R^3$		$25500/R^5$
321	32-2					$25500/R^5$
32-1	32-1			$126.0/R^3$		$25500/R^5$
32-1	322					$25500/R^5$
32-1	32-2			$126.0/R^3$		$25500/R^5$
322	322			$126.0/R^3$		$25500/R^5$
322	32-2					$25500/R^5$
32-2	32-2			$126.0/R^3$		$25500/R^5$

TABLE BIII. Asymtotic radial dependence of the V(t) matrix elements for the n = 3 levels

$n\ell_1 m_1$	$n\ell_3 m_3$	2^0-pole	2^1-pole	2^2-pole	2^3-pole	2^4-pole
300	300					
300	310		$-12.73/R^2$			
300	311		$-12.73/R^2$			
300	31-1		$-12.73/R^2$			
300	320			$142.3/R^3$		
300	321			$142.3/R^3$		
300	32-1			$142.3/R^3$		
300	322			$142.3/R^3$		
300	32-2			$142.3/R^3$		
310	310			$180.0/R^3$		
310	311			$180.0/R^3$		
310	31-1			$180.0/R^3$		
310	320		$-10.06/R^2$		$-2112.0/R^4$	
310	321		$-10.06/R^2$		$-2112.0/R^4$	
310	32-1		$-10.06/R^2$		$-2112.0/R^4$	
310	322				$-2112.0/R^4$	
310	32-2				$-2112.0/R^4$	
311	311			$180.0/R^3$		
311	31-1			$180.0/R^3$		
311	320		$-10.06/R^2$		$-2112.0/R^4$	
311	321		$-10.06/R^2$		$-2112.0/R^4$	
311	32-1				$-2112.0/R^4$	
311	322		$-10.06/R^2$		$-2112.0/R^4$	
311	32-2				$-2112.0/R^4$	

APPENDIX C

CALCULATIONS BASED ON THE SHEN-COOPER FORMALISM

We consider here the calculation of the impact broadening operator ϕ based on the development by Shen and Cooper[34]. This formalism, in effect replaces Eq. (10), which can be written as a time ordered exponential, by the exponential; the assumption being that $V(t_1)$ commutes with $V(t_2)$. When applied to the $n' = 2$ levels one obtains results essentially equivalent to those of Griem[20]. The formalism is easily applied to levels other than those with $n' = 2$ and effectively sums the complete series (Eq. 10) with the assumption mentioned above. The development by Griem[20] though formally equivalent is less adaptable to other levels. Also the formalism of Shen and Cooper is readily extendable to the two state case (i.e., upper and lower state broadening). These calculations are relatively easy to perform and provide useful cross checks amongst the various calculations. In addition compared with the "dipole only" calculations of Section III indicates the effects of correct time ordering in the higher order terms of the Dyson expansion.

Two State Case

Expressing the S-matrices in the collision axes (S_{nc}), one may transform the fixed atomic axes into the collision axes by a rotation through the Euler Angles. The final angular average is then obtained by averaging over all the Euler angles since the collisions occur at random directions. The resulting average

may be written(see also reference 6),

$$\ll n\ell_1 m_1; n'\ell_2 m_2 | \{S_3^* S_2 - 1\}_{AV.} | n'\ell_4 m_4; n\ell_3 m_3 \gg = \sum_{\substack{m_1' m_3' \\ m_2' m_4'}} (-1)^{m_4 - m_4' + m_1 - m_1'}$$

$$\times \sum_{\ell} (2\ell+1) \begin{pmatrix} \ell_1 & \ell_3 & \ell \\ -m_1' & m_3' & (m_1' - m_3') \end{pmatrix} \begin{pmatrix} \ell_1 & \ell_3 & \ell \\ -m_1 & m_3 & (m_1 - m_3) \end{pmatrix}$$

$$\times \begin{pmatrix} \ell_2 & \ell_4 & \ell \\ -m_2' & m_4' & (m_2' - m_4') \end{pmatrix} \begin{pmatrix} \ell_2 & \ell_4 & \ell \\ -m_2 & m_4 & (m_2 - m_4) \end{pmatrix} \delta_{(m_1' - m_3')(m_4' - m_3')} \qquad \text{(C1)}$$

$$\times \delta_{(m_1 - m_3)(m_4 - m_3)} \left\{ \langle \ell_1 m_1' | S_{3c}^* | \ell_3 m_3' \rangle \langle \ell_2 m_2' | S_{2c} | \ell_4 m_4' \rangle - \delta_{\ell_1 \ell_3} \delta_{m_1' m_3'} \delta_{\ell_2 \ell_4} \delta_{m_2' m_4'} \right\}$$

The matrix elements of $\langle \ell_1 m_1' | S_{3c}^* | \ell_3 m_3' \rangle$ and $\langle \ell_2 m_2' | S_{2c} | \ell_4 m_4' \rangle$ have forms similar to Eq. (13) of Reference 39. Inspection indicates that the average in the two state case will consist of a sum of cosines involving sums and differences of the arguments of the "n = 3 cosines" and the "n = 2 cosines" (see Shen and Cooper[34]). In fact we may conveniently express the matrix elements in the following form

$$\ll n\ell_1 m_1; n'\ell_2 m_2 | \{S_3^* S_2 - 1\}_{AV.} | n'\ell_4 m_4; n\ell_3 m_3 \gg =$$

$$\left\{ \sum_{i=1}^{6} 2V_i [\cos(3i/\rho) - 1] \right\} + 2V_7 [\cos(24/\rho) - 1] \qquad \text{(C2)}$$

where ρ is in units of $\hbar/mv$. In Table C1 we have tabulated the relevant non zero matrix elements of $\{S_3^* S_2 - 1\}$, according to the format Eqs. (C2). These were obtained using the IBM 7094 computer to evaluate Eq. (C1) using Eq. (13) of Reference 34 for the matrix elements of S_{3c}^* and S_{2c}. The matrix $\{S_3^* S_2 - 1\}_{av.}$ is symmetric and hence only the diagonal elements and half the off diagonal elements are given. Furthermore elements with negative m's are not shown since they are equal to those with positive m. Keeping the 1st two terms of the cosines in Eq. (C2)

TABLE CI. Values of the V's (Eq. C2) for the $\{S_3^* S_2 - 1\}_{av.}$ matrix elements using the formalism of SC applied to the two-state case.

$n\ell_1 m_1$	$n'\ell_2 m_2$	$n'\ell_4 m_4$	$n\ell_3 m_3$	V_1	V_2	V_3	V_4	V_5	V_6	V_7	$2\mathcal{H}/3$
300	200	200	300		.1667		.1667			.1667	126.0
310	200	200	310	.1667			.0833	.1667		.0833	99.0
311	200	200	311	.1667			.0833	.1667		.0833	99.0
320	200	200	320	.1000	.2667		.0167	.1000		.0167	45.0
321	200	200	321	.1000	.2667		.0167	.1000		.0167	45.0
300	200	210	310				.0680			-.0680	- 29.4
310	200	210	300				.0680			-.0680	- 29.4
310	200	210	320	.0577			.0193	-.0578		-.0193	- 20.8
311	200	210	321	.0500			.0167	-.0500		-.0167	- 18.0
320	200	210	310	.0577			.0193	-.0578		-.0193	- 20.8
321	200	210	311	.0500			.0167	-.0500		-.0167	- 18.0
311	200	211	300				.0680			-.0680	- 29.4
311	200	211	320	-.0289			-.0096	.0289		.0096	10.4
321	200	211	310	.0500			.0167	-.0500		-.0167	- 18.0
300	210	210	300		.0556		.0556		.2222	.0556	114.0
310	210	210	310	.0333		.2667	.0500	.0333	.0667	.0500	87.0
311	210	210	311	.0667		.2000	.0167	.0667	.1333	.0167	87.0
320	210	210	320	.0429	.0635	.1143	.0087	.0429	.0159	.0087	33.0
321	210	210	321	.0381	.0762	.1238	.0071	.0381	.0191	.0071	33.0
300	211	211	300		.0556		.0556		.2222	.0556	114.0
310	211	211	310	.0667		.2000	.0167	.0667	.1333	.0167	87.0
311	211	211	311	.0500		.2333	.0333	.0500	.1000	.0333	87.0
320	211	211	320	.0286	.1016	.1429	.0040	.0286	.0256	.0040	33.0
321	211	211	321	.0310	.0952	.1381	.0048	.0310	.0238	.0048	33.0
322	211	211	322	.0381	.0762	.1238	.0071	.0381	.0191	.0071	33.0

TABLE CII. Additional $\{S_3^* S_2 - 1\}_{av.}$ matrix elements which go to zero for large impact parameters

$n\ell_1 m_1$	$n'\ell_2 m_2$	$n''\ell_4 m_4$	$n\ell_3 m_3$	V_1	V_2	V_3	V_4	V_5	V_6	V_7	$2\sqrt{3}$
300	210	210	320		-.0314		.0157		-.0314	.0157	0
311	210	211	310	-.0167		.0333	.0167	-.0167	-.0333	.0167	0
321	210	211	300		-.0272		.0136		-.0272	.0136	0
321	210	211	320	.0041	-.0110	-.0082	.0014	.0041	-.0028	.0014	0
300	211	211	320		.0157		-.0079		.0157	-.0079	0

one obtains[34]

$$2[r_3\cdot r_3 + r_2\cdot r_2 - 2r_3\cdot r_2]/3\rho^2 \equiv 2Q/3\rho^2$$

Column 12 shows the values of 2/3 Q thus obtained. These may be checked by applying the doubled transformation of Appendix A to the $[r_3\cdot r_3+r_2\cdot r_2-2r_3\cdot r_2]$ matrix elements given in Reference 3. In column 5, Table I of Section IV are listed the values of the constant K which appears in Eq. (20) of Section II. The constant K may be shown to be given by,

$$K_{ij} = 3\sum_{\ell=1}^{4} V_\ell(3\ell)^2[2K(3\ell) - 1.846 + \ln\{27\ell^2/2n^4\}]/2Q$$
$$+3V_7(24)^2[2K(24) - 1.846 + \ln\{3(24)^2/2n^4\}]/2Q \qquad \text{(C3)}$$

where the V 's are given in Table C1 and

$$K(i) = \sin i/i - \cos i/i^2 + 1/i^2 - Ci(i)$$

$C_i(i)$ is the usual cosine integral. This form for the constant K is valid provided

$$24(m/kT_2)^{1/2}k/m\rho_D \ll 1 \qquad \text{(C4)}$$

and may be derived with the help of Eq. (21) of Reference 34. The condition (C4) is the condition Eq. (20) of Reference 34 and provides a limiting condition on electron density N and temperature T for which K is given by (C3). Table CII lists additional elements which are zero in the limit ρ large (i.e., in the limit that it is sufficient to retain only the 1st two terms of the cosines).

The matrix elements from rows 20, 21, 23 and 25 plotted as a function of ρ (in units of $\hbar/mv$) are shown in Figs. (4), (5), (6), and (7) of SectionIV. The first three of these elements apply to the weaker of the two unshifted components of the Stark pattern (see Eq. 22 of SectionIII) while the latter applies to the strongest unshifted components. Similar curves for the other $\{S_3^* S_2 - 1\}_{av.}$ elements may be plotted using the V's of Table CII and Eq. (C1).

UNCLASSIFIED

Security Classification

DOCUMENT CONTROL DATA - R & D

(Security classification of title, body of abstract and indexing annotation must be entered when the overall report is classified)

1. ORIGINATING ACTIVITY *(Corporate author)*
Plasma Physics Research Laboratory
Air Force Systems Command
Wright-Patterson AFB, Ohio 45433

2a. REPORT SECURITY CLASSIFICATION
UNCLASSIFIED

2b. GROUP

3. REPORT TITLE
Classical Path Calculations of the Impact Broadening Operator for the Stark Broadening of H_α

4. DESCRIPTIVE NOTES *(Type of report and inclusive dates)*
Scientific, Final.

5. AUTHOR(S) *(First name, middle initial, last name)*
M. E. Bacon

6. REPORT DATE	7a. TOTAL NO. OF PAGES	7b. NO. OF REFS
December 1970	74	37

8a. CONTRACT OR GRANT NO.

b. PROJECT NO. 7073 00 01

c. DOD Element 61102F

d. DOD Sub-Element 681301

9a. ORIGINATOR'S REPORT NUMBER(S)

9b. OTHER REPORT NO(S) *(Any other numbers that may be assigned this report)*
ARL 70-0276

10. DISTRIBUTION STATEMENT
This document has been approved for public release and sale; its distribution is unlimited.

11. SUPPLEMENTARY NOTES
TECH OTHER

12. SPONSORING MILITARY ACTIVITY
Aerospace Research Laboratories (LU)
Air Force Systems Command
Wright-Patterson AFB, Ohio 45433

13. ABSTRACT

Previous classical path calculations of the impact-broadening operator (ϕ) for the Stark broadening of the hydrogen line H_α are reviewed. ϕ is then computed by solving numerically for the S-matrices using the straight-line-classical path approximation. All contributing mutipoles in the perturber-atom interaction V(t) are included and time ordering of the operators in the S-matrices is retained. The resulting ϕ matrix elements are compared with the previous approximations. The effects on the H_α line profile are considered.

DD FORM 1 NOV 65 1473

UNCLASSIFIED

Security Classification

14 KEY WORDS	LINK A		LINK B		LINK C	
	ROLE	WT	ROLE	WT	ROLE	WT
Line Broadening Stark Effect Plasma Spectroscopy						